Julius-Maximilians-Universität Würzburg

Functional analysis of polarization and podosome formation
of murine and human megakaryocytes

Funktionale Untersuchungen der Polarisation und
Podosomenbildung muriner und humaner Megakaryozyten

Doctoral thesis for a medical doctoral degree
at the Graduate School of Life Sciences
Section Biomedicine

submitted by

Frank Gerner

from

Hanau

Würzburg, 2017

Members of the *Promotionskomitee*:

Chairperson: Professor Dr. Cynthia Sharma

Primary Supervisor: Professor Dr. Bernhard Nieswandt

Supervisor (Second): Professor Dr. Katrin Heinze

Supervisor (Third): Professor Dr. Christoph Kleinschnitz

Supervisor (Fourth): Professor Dr. Antje Gohla

Date of Public Defence: _____

Date of Receipt of Certificates: _____

Summary

In mammals, blood platelets are produced by large bone marrow (BM) precursor cells, megakaryocytes (MK) that extend polarized cell protrusions (proplateles) into BM sinusoids. Proplatelet formation (PPF) requires substantial cytoskeletal rearrangements that have been shown to involve the formation of podosomes, filamentous actin (F-actin) and integrin-rich structures. However, the exact molecular mechanisms regulating MK podosome formation, polarization and migration within the BM are poorly defined. According to current knowledge obtained from studies with other cell types, these processes are regulated by Rho GTPase proteins like RhoA and Cdc42.

In this thesis, polarization and podosome formation were investigated in MKs from genetically modified mice, as well as the cell lines K562 and Meg01 by pharmacological modulation of signaling pathways.

The first part of this thesis describes establishment of the basic assays for investigation of MK polarization. Initial data on polarization of the MK-like erythroleukemia cell line K562 revealed first insights into actin and tubulin dynamics of wild type (WT) and RhoA knock-out ($RhoA^{-/-}$) K562 cells. Phorbol 12-myristate 13-acetate (PMA)-induction of K562 cells led to the expected MK-receptor upregulation but also RhoA depletion and altered polarization patterns.

The second part of this thesis focuses on podosome formation of MKs. RhoA is shown to be dispensable for podosome formation. Cdc42 is revealed as an important, but not essential regulator of MK spreading and podosome formation. Studies of signaling pathways of podosome formation reveal the importance of the tyrosine kinases Src, Syk, as well as glycoprotein (GP)VI in MK spreading and podosome formation.

This thesis provides novel insights into the mechanisms underlying polarization and podosome formation of MKs and reveals new, important information about cytoskeletal dynamics of MKs and potentially also platelets.

Zusammenfassung

Bei Säugetieren entstehen Blutplättchen aus großen Knochenmark-vorläuferzellen, Megakaryozyten, die lange, polarisierte Zellprotrusionen (Proplättchen) in Knochenmarkssinusoide ausstülpen. Die Bildung von Proplättchen erfordert eine umfangreiche Reorganisation des Zytoskeletts, die die Bildung von Podosomen, F-Aktin- und Integrinreichen Strukturen beinhaltet. Die genauen molekularen Mechanismen, die megakaryozytäre Podosomenbildung, Polarisation und Migration im Knochenmark regulieren, sind jedoch bisher unzureichend erforscht. Rho GTPasen wie beispielsweise RhoA und Cdc42 sind nachgewiesenermaßen beteiligt an der klassischen Zytoskelettregulierung.

In dieser Dissertation wurden die obengenannten Reifungsprozesse mithilfe von Megakaryozyten von genetisch modifizierten Mäusen sowie den Zelllinien K562 und Meg01 durch pharmakologische Beeinflussung zellulärer Signaltransmitter erforscht.

Im ersten Teil der Dissertation wurden Experimente zur Untersuchung megakaryozytärer Polarisation etabliert. Initiale Daten über die Polarisation der megakaryozytären, erythroleukämischen Zelllinie K562 erlaubten Einblicke in Aktin- und Tubulindynamik von Wildtyp- und RhoA-defizienten K562 Zellen. Phorbol-12-myristat-13-acetat (PMA)-induzierte K562-Differenzierung verursachte die erwartete Hochregulierung megakaryozytärer Rezeptoren, aber auch eine unerwartete RhoA-Depletion und bisher unbeobachtete Polarisationsmuster. Der zweite Teil dieser Dissertation galt der Untersuchung der Podosomenbildung von Megakaryozyten. RhoA zeigte sich als entbehrlich für die Podosomenbildung, während Cdc42 sich als wichtiger, dennoch nicht essentieller Regulator der podosomenbildenden Zytoskelettdynamik erwies. Untersuchungen von Signalwegen in der Podosomenbildung von Megakaryozyten offenbarten die Bedeutung von Tyrosinkinasen Src, Syk sowie Glykoprotein VI bei der MK-Adhäsion und der Bildung von Podosomen.

Somit liefert diese Dissertation neue Einblicke in die Signalwege der dynamischen Regulation des Zytoskeletts in Megakaryozyten.

Table of contents

1 INTRODUCTION

1.1 Platelets

With a diameter of 2 - 3 μm in humans and 1 - 1.5 μm in mice, platelets are the smallest cells circulating in the blood system of mammals. These anucleated, discoid-shaped cells remain in human blood for up to 10 days at a concentration of 150,000 - 350,000/ml and in murine blood for up to 5 days at a concentration of approximately 450,000 - 1,690,000/ml[1]. Aged platelets are constantly removed by macrophages in the spleen and liver. As a result of their short life span, every day, BM-derived MKs release approximately $1x10^{11}$ platelets into the blood stream in order to maintain a stable blood platelet count[2]. This process is referred to as megakaryopoiesis.

Platelets are pivotal for primary hemostasis. Physiological plug formation is achieved by shape change, adhesion and aggregation of platelets, which become activated by extracellular matrix (ECM) components that are exposed upon vessel injury[3]. Defects in the process of megakaryopoiesis and platelet release can lead to pathological, life-threatening conditions; increased coagulability, disturbed blood flow and endothelial cell injury are risk factors for a vessel occluding process called thrombosis[4]. Further, malfunction or a reduced number of platelets may result in bleeding disorders. In addition to their well-known function in hemostasis and thrombosis, platelets also participate in embryonic vascular development[5], wound healing[6], inflammatory responses[7] and tumor metastasis[8].

1.2 MKs – the platelet precursors

MKs are large platelet precursor cells which are predominantly located in the BM[9], but also in the spleen[10] and the lungs[11]. Mature MKs (myeloid cells) derive from pluripotent long term hematopoietic stem cells (LT-HSCs), which are capable of producing the whole spectrum of different blood cells (Figure 1).
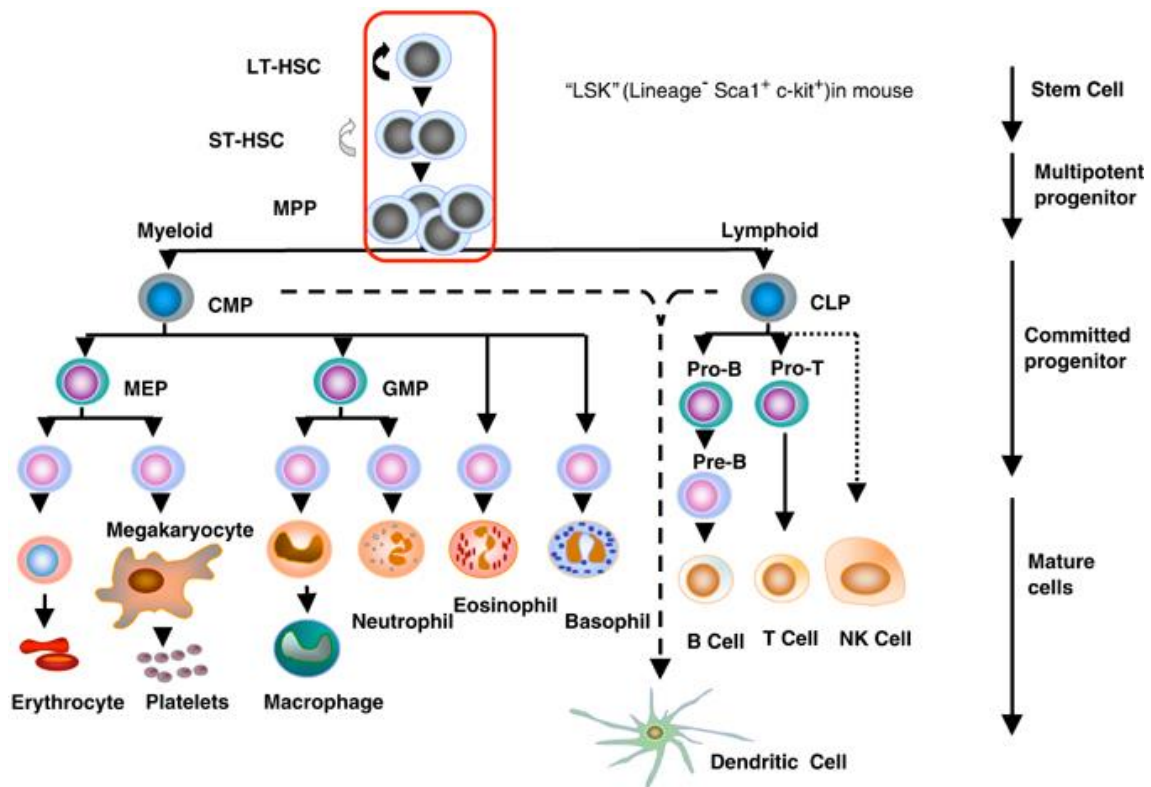
Figure 1: Hematopoietic cell differentiation.
LT-HSCs undergo mitosis to enable sufficient supply of MPPs for a stable level of all blood cells. Triggered by certain erythrocyte- and/or platelet-associated cytokine signals, MPPs differentiate to CMPs, and later to MEPs of the myeloid development branch. In their final differentiation step, MEPs finally advance either to erythrocytes or to MKs and platelets.
Abbreviations: HSC = hematopoietic stem cell; LT-HSC = long-term repopulating HSC; ST-HSC = short-term repopulating HSC; MPP = multipotent progenitor; CMP = common myeloid progenitor; CLP = common lymphoid progenitor; MEP = MK/erythroid progenitor; GMP = granulocyte-macrophage progenitor.

Taken from: Larsson & Karlsson, Oncogene, 2005[12]

In order to become mature and specialized for platelet production, MKs pass through different stages of development (Figure 2). Proliferation of burst- or colony-forming unit MKs (BFU/CFU-MKs) serves to increase the number of MK progenitors - promegakaryoblasts (PMKB). By losing the ability of classical mitosis, PMKBs start to amplify the DNA content of the cell up to a ploidy of 64N in humans and 128N in mice (modal ploidy of 16N in human and mice) by undergoing several rounds of endomitosis (endoreplication). Final maturation of MKs is characterized by cytoplasmic development. Growth and synthesis of platelet-specific organelles are major hallmarks of this process, which enables

MKs to reach a size of up to 60 µm in humans and approximately 20-30 µm[13] in mice.
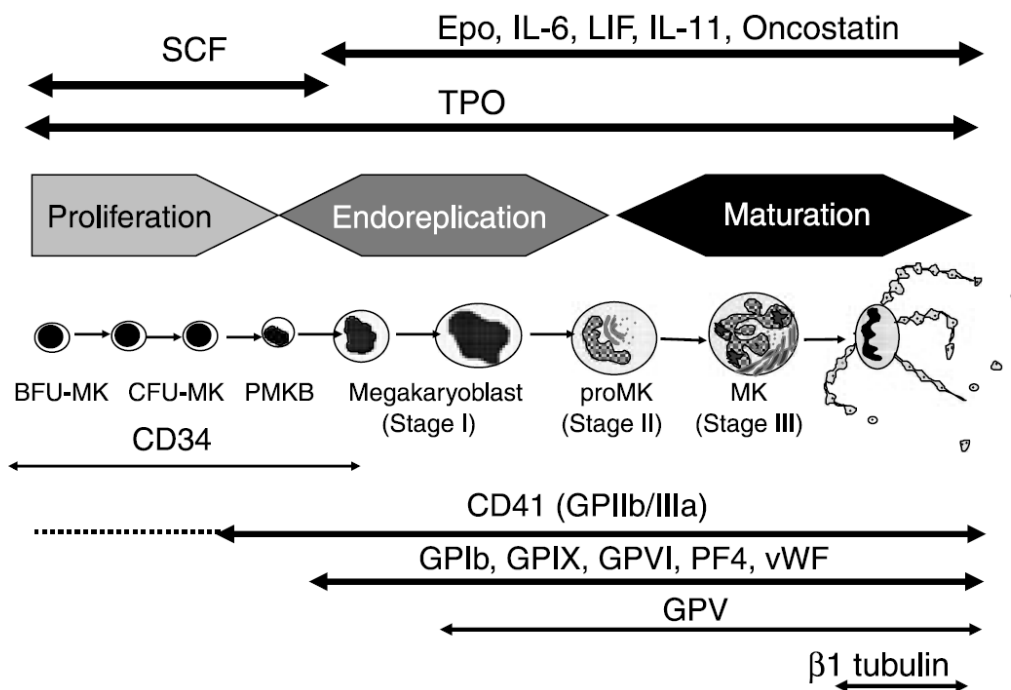
Figure 2: MK maturation.
This overview shows the final differentiation steps in MK maturation from BFU-MKs to proplatelet forming MKs (displayed in the middle) and important required cytokines (displayed at the top), as well as differentiation markers (displayed at the bottom).
<u>Abbreviations</u>: SCF = stem cell factor; TPO = thrombopoietin; Epo = erythropoietin; IL = interleukin; LIF = leukemia inhibitory factor; BFU-MK = burst forming unit MK; CFU-MK = colony forming unit MK; PMKB = promegakaryoblast; CD = cluster of differentiation; GP = glycoprotein; PF = platelet factor; vWF = von Willebrand factor.

Taken from: Chang et al., JTH, 2007[14]

According to current knowledge, it is presumed, that thrombopoietin (TPO) is the primary regulator of megakaryopoiesis and thrombopoiesis. However, it does not seem to be sufficient but acts in concert with many other cytokines, such as stem cell factor (SCF), erythropoietin (Epo), interleukin 6 and 11 (IL-6 and IL-11), leukemia inhibitory factor (LIF) and oncostatin[14].

1.3 Bone marrow function and extracellular matrix components

The bone matrix is divided into two macroscopic distinct tissues: solid bone and BM. Solid bone (S*ubstantia compacta*), consisting of minerals (hydroxylapatite-crystals; 45%), organic material (cells and ECM; 35%) and water (25%), provides the outer casing of the bone. Cancellated bone (*Substantia spongiosa*) is much less densely packed and consists of solid trabeculae, building up meshes that hold the BM (Medulla ossium; site of hematopoiesis) inside. Finally, the periost covers all outer parts of the bone while the endost covers inner bone parts.

The BM is a soft tissue located inside of the bones and can be further subdivided into two compartments: yellow and red BM. Yellow BM consists mainly of fat cells (adipocytes) and reticular cells. It lacks the ability of hematopoiesis. The red BM is the site of hematopoiesis and provides space for a large number of different cells in all stages of maturation: erythrocytes, lymphocytes, MKs, monocytes and granulocytes. The infrastructure-maintaining fraction is built up by fat cells, macrophages, endothelial cells (building up sinusoids), as well as the reticular connective tissue which consists of fibroblastic reticular cells and reticular fibers. Reticular fibers are made of a complex composition of ECM molecules (collagen fibrils type I, III, IV and VI, elastin, fibrillin-microfibrils, fibrinogen, fibronectin, laminins, perlecans and proteoglycans). They build up a three-dimensional meshwork (partially coated by fibroblastic reticulum cell extensions) providing space and stability for the upper mentioned cells[15,16]. All components of the ECM appear in definite, site-specific concentrations in the BM.

1.4 MK migration, polarization and podosome formation

It was for a long time presumed that during and/or after maturation, MKs migrate from the BM osteoblastic niche, which predominantly contains PPF inhibiting collagen, towards the vascular niche, which is containing PPF inducing molecules such as von Willebrand factor[17,18]. To date unconfirmed theories claim a high gradient of the cytokine stromal-cell derived factor 1α (SDF-1α) (Figure 3A) as the trigger for this migration. Furthermore, SDF-1α plays a major role in embryogenesis[19,20], angiogenesis[21], as well as lymphocyte[22] and macrophage recruitment[23].
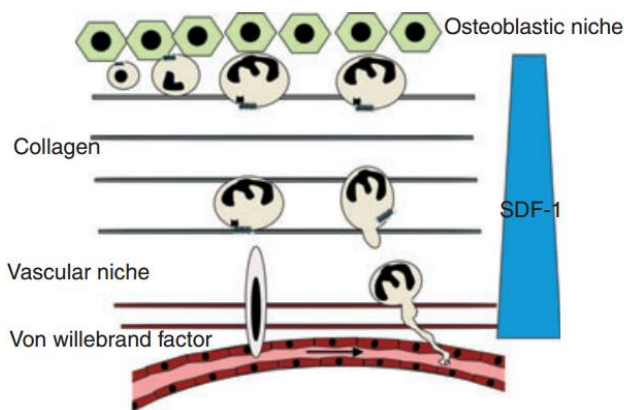
Figure 3 A: Old model of MK migration.
MK maturation initiates at sites of the osteoblastic niche. Here, proplatelet inhibiting collagen dominates the ECM-composition. After final maturation, MKs migrate from the osteoblastic niche towards the vascular niche, directed by a high SDF-1 gradient. Von Willebrand factor induces platelet release. This is accomplished either by migration of entire MKs through the endothelial barrier (bottom left) or by protrusion of long proplatelet extensions (bottom right) into the vessel lumen. Finally, the shear force of the blood flow sheds down proplatelets and platelets are released into the blood.
Abbreviations: SDF-1 = stromal-cell derived factor 1.

Taken from: Bluteau et al., JTH, 2009[24]

Contradicting the "MK migration hypothesis", it was recently shown that the BM does not provide enough space for MK migration, and thus suggests polarization as the major mechanism by which mature MKs localize next to sinusoids[25] (Figure 3B).
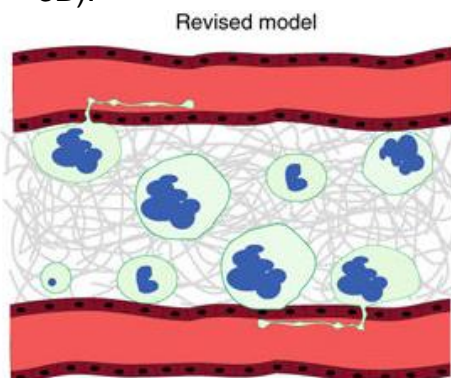
Figure 3 B: Revised model: Thrombopoiesis is spatially regulated by the BM vasculature.
Recent data support a model where, due to space limitations in the BM, all MKs reside close to sinusoids and are replenished by precursors originating from the sinusoidal niche rather than a periostic niche.

Taken from: Stegner et al., Nat. Commun. 2017[25]

Upon contact with the sinusoidal vessel, it is supposed that MKs form polarized proplatelet protrusions, triggered by a spingosine-1-phosphate (S1P) gradient[26]. S1P can be detected by MKs through their highly expressed sphingosine-1-phosphate receptor 1 (S1P1), which induces G_i proteins. This leads to the activation of PI-3-kinase (PI3K), phospholipase C (PLC) and Ras GTPase signaling pathways which induce protrusion formation and platelet release. Under physiological conditions, PPF is unilaterally built up into the direction of the vessel wall (Figure 4).
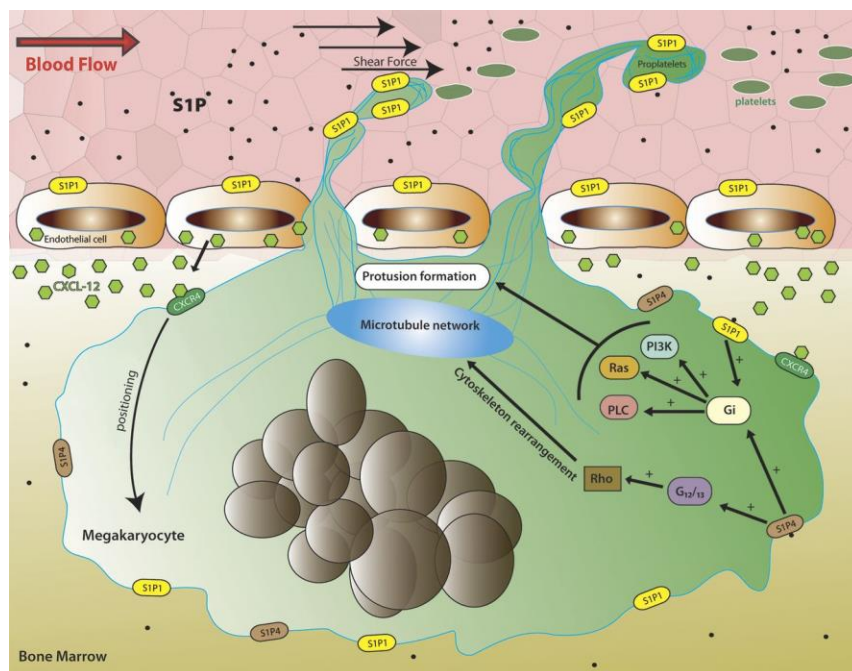
Figure 4: Model of proplatelet polarization into the blood vessel.
S1P-triggered activation of S1P1 activates G_i protein, phospholipase C (PLC), Ras GTPase and PI-3-kinase (PI3K) and thus initiate cytoskeleton rearrangement of actin and microtubulin. Proplatelet extensions into the sinusoidal vessels are thought to be directed by a high gradient of S1P inside the vessel lumen.
Abbreviations: S1P = sphingosine-1-phospate; S1P1 = sphingosine-1-phosphate receptor 1; CXCL-12 = CXC-motive-chemokine 12; CXCR-4 = CXC-motive-chemokine receptor 4; S1P4 = sphingosine-1-phosphate receptor 4; G_i = G_i protein-coupled receptor; PI3K = phosphoinositide 3-kinase; Ras = ras protein; PLC = phospholipase C; $G_{12/13}$ = subunits of G-protein coupled receptors; Rho = rho GTPase family proteins.

Taken from: Hla et al., J Exp Med, 2012[27]

A current hypothesis proposes that podosomes, formed in response to interaction with components of the sinusoidal vessel wall, are involved in the initiation of PPF. Podosomes are subcellular actin-rich structures of approximately 0.5 - 2 µm

size and consist of an actin-rich core and an adhesion ring. They seem to be closely related 'focal adhesions' which function as mechanical linkages to the ECM and as biochemical signaling hubs[28]. Further, podosomes possess the ability to degrade ECM components[29].

Podosome formation is a complex process triggered by cytokines (e.g. SDF-1α), growth factors (e.g. tumor necrosis factor alpha (TNF-α) and transforming growth factor beta (TGF-β)), as well as ECM components, which can be bound by glycoprotein receptors, tyrosine kinase receptors and integrins. Downstream of these receptors, internal signaling cascades, including GTP exchange factors (GEFs), protein kinase C (PKC) and Src-family tyrosine kinase (Src) further activate secondary effectors like small GTPase proteins of the Rho-family: Rac1, RhoA and Cdc42. These secondary effectors in turn regulate several terminal effectors (focal adhesion proteins, actin and myosin), which contribute to podosome formation[29,30].

This interplay of cytoskeletal proteins (Arp2/3, WASp and cortactin) with adhesion proteins and myosin driven contractility causes, among other functions, classical arrangement of podosomes[30]. In different experimental approaches podosomes were shown to either appear as distinct structures, or as part of superstructures (rosettes, belts or clusters[28]).

MKs can degrade ECM and basement membrane of sinusoids via secreted matrix metalloproteinases (MMPs) (Figure 5 bottom left) and thus gain direct access to the vascular system. Proplatelets can then protrude into the vessel lumen and are shed off and further fragmented by the blood shear forces until finally becoming platelets (Figure 5). Whether direct interaction between podosomes and proplatelets exist, is currently not established (Figure 5 bottom right).

Formation of podosomes, characterized by a flat and sparsely invasive appearance, can be observed in many different physiological cell types. Strongly invasive invadopodia (together with podosomes belonging to the family of invadosomes) are predominantly found in cell lines derived from cancer cells[31,32].
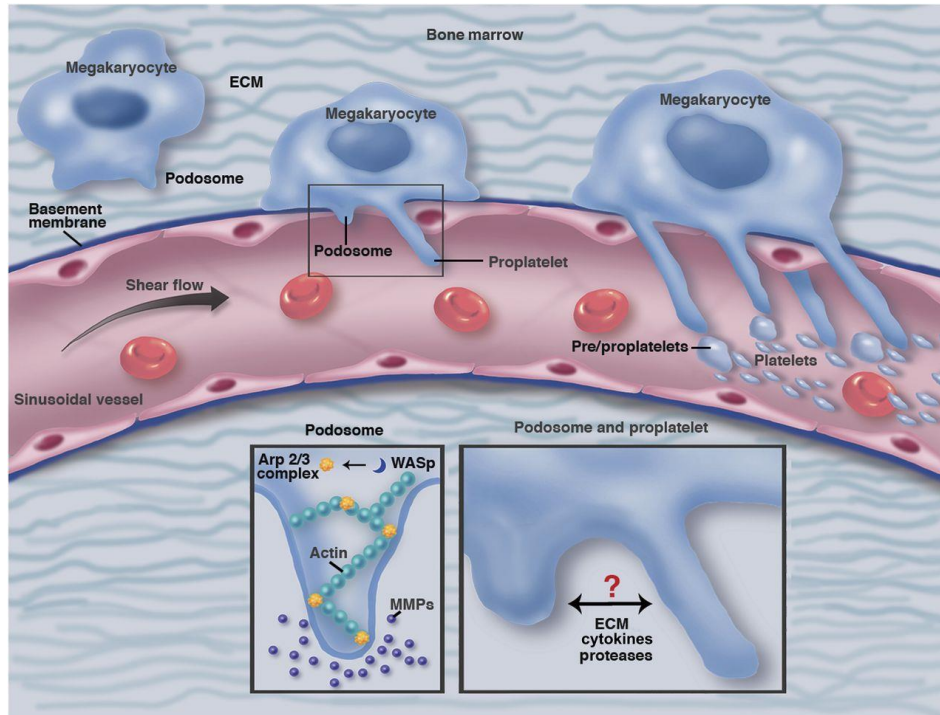
Figure 5: Model of podosome formation in MKs.
BM-derived MKs transmigrate through the BM ECM to access the basement membrane of sinusoidal vessels. It is hypothesized that WASp and Arp2/3 activate actin rearrangement and thus the formation of podosomes. MMPs is secreted and degrades the membrane. Thereby, MKs gain access to the vessel lumen. Shear forces of the blood inside the vessel are proposed to shed these pre/proplatelets and facilitate their maturation into final platelets. The relationship of podosomes and proplatelets still remains to be investigated.
Abbreviations: ECM = extracellular matrix; WASp = Wiscott-Aldrich syndrome protein; MMPs = matrix metalloproteinases.

Taken from: French DL, Blood, 2013[33]; Professional illustration by Marie Dauenheimer.

As the current knowledge about podosome formation in MKs is almost exclusively based on data of *in vitro* experiments, the relevance of these findings for the actual *in vivo* situation remains to be investigated. Additionally, signaling molecules, participating in podosome formation in MKs still have to be revealed.

1.5 The Rho family of small GTPases

The Rho family of small GTPases is a subfamily of the Ras superfamily, which includes different small signaling proteins with a size of 20-25 kDa[34]. They are constitutively expressed and serve as binary molecular switches[35]. The main function of the Rho GTPases is the regulation of actin and microtubule dynamics, which are crucial for cytoskeleton-dependent processes like mitosis, migration, polarization and also podosome formation. Rho GTPases additionally have regulative function in cellular gene transcription[35].

The Rho family includes 23 different Rho GTPases, which are further divided into 6 subclasses[36] (Figure 6). To date, Cdc42, Rac1 and RhoA have been most intensively studied.
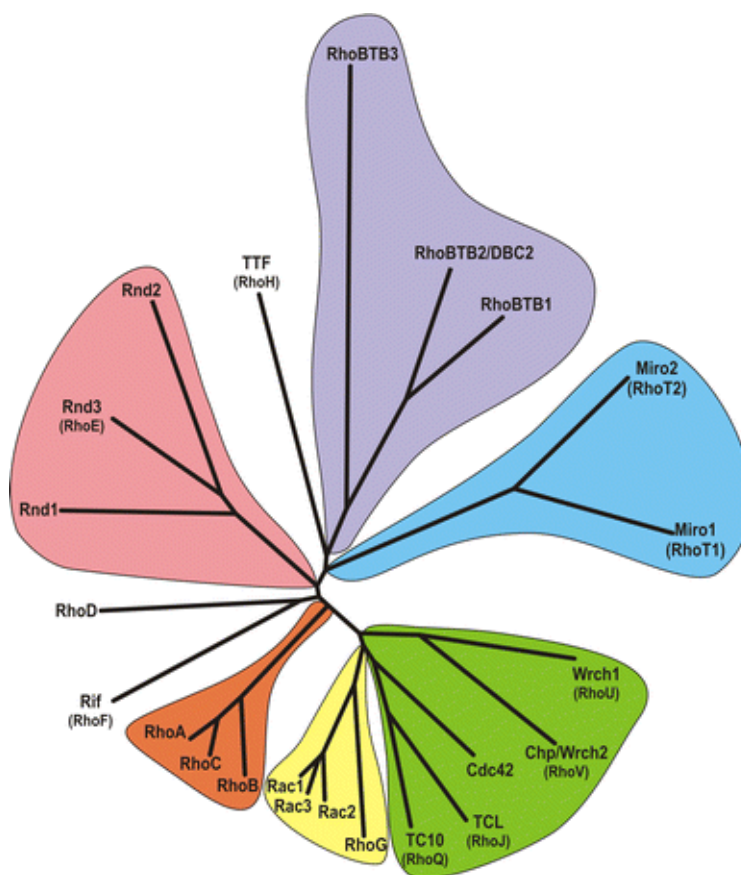
Figure 6: Dendrogramm of the family of small Rho GTPases.
All 23 members of the family of small Rho GTPases and their relationship are displayed. Rho GTPase subfamilies are highlighted in different colored shapes: RhoBTB (purple), Miro (light blue), Cdc42 (green), Rac (yellow), RhoA (orange) and Rnd (pink). Brackets provide alternative names of these proteins. Phylogenetic analysis was performed using ClustalW with protein sequences obtained from the NCBI database and illustrated by TreeView.

Taken from : Ellenbroek et al.; Clin Exp Metastasis; 2007[36]

The activity of proteins of the Rho family is controlled and regulated by guanine nucleotide dissociation inhibitors (GDIs), guanine nucleotide exchange factors (GEFs) and GTPase-activating proteins (GAPs). GDIs enable inactive, GDP-bound, Rho proteins to remain in a cytoplasmic state by hiding their C-terminal

tail, which is required for membrane colocalization. As soon as Rho proteins dissociate from their GDIs, they translocate to the cellular plasma membrane and establish contact with different ligand-receptor systems, such as integrins, G-protein coupled receptors and receptor tyrosine kinases. Stimulating these receptors initiates binding of Rho proteins to GEFs, which furthermore phosphorylate Rho proteins. This activates downstream effectors, which further regulate cytoskeletal organization, gene transcription, apoptosis or membrane transport. Rho protein deactivation is accomplished by re-exchanging GTP to GDP through intrinsic GTPase activity, stimulated by GAPs[36] (Figure 7).
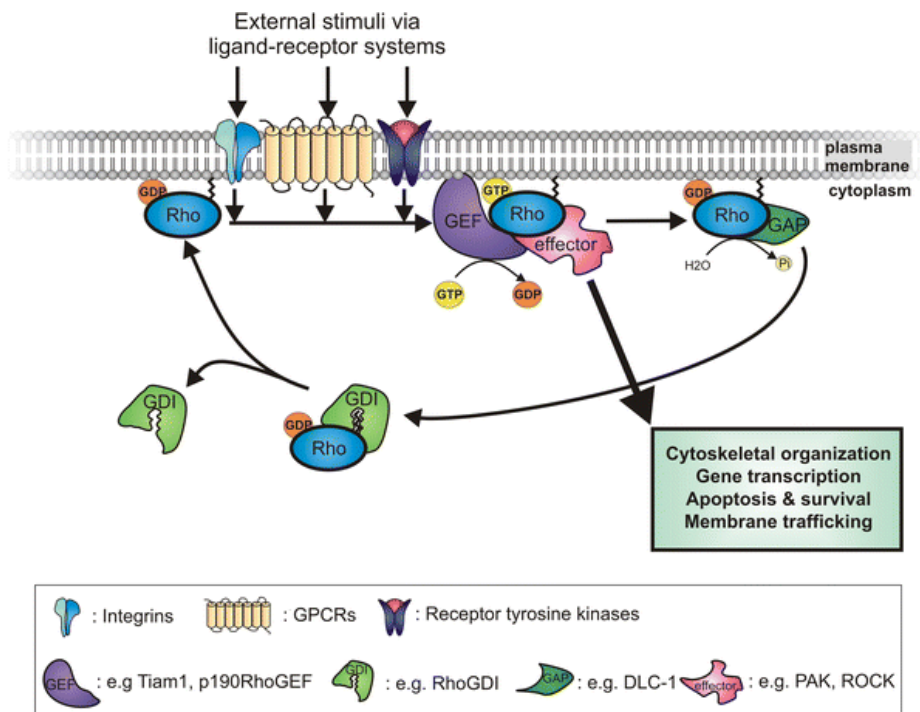
Figure 7: Regulation of the GTPase cycle.
Inactivated Rho GTPases remain in the cytoplasm until becoming activated through GDI dissociation. Upon external stimuli via ligand-receptor systems (integrins, G-protein coupled receptors or receptor tyrosine kinases) GEFs connect to the now plasma-membrane-bound Rho-GTPase. Transformation of GTP to GDP supplies energy for effector activation. GAPs then inactivate Rho-GTPases again, leading to dissociation from the plasma membrane and association with GDIs.
Abbreviations: GDP = guanosine diphosphate; GTP = guanosine triphosphate; GDI = guanine nucleotide dissociation inhibitor; GEF = guanine nucleotide exchange factor; GAP = GTPase-activating proteins; GPCR = G-protein-coupled receptor

Taken From: Ellenbroek et al.; Clin Exp Metastasis; 2007[36]

1.5.1 Ras homolog gene family member A (RhoA)

RhoA is a small Rho GTPase protein with a molecular weight of 22 kDa. It belongs to the Rho subclass, which consists of RhoA, RhoB and RhoC[36]. According to current knowledge, RhoA is considered a major player in the regulation of important actin cytoskeleton dynamics like formation of focal adhesions and stress fibers[37]. Constitutive RhoA knockout mice do not survive early stages of embryonic development[37]. Conditional gene knockout of RhoA in platelets and MKs in mice causes macrothrombocytopenia, although platelet life span is only mildly reduced, indicating a platelet production defect. Furthermore, RhoA-deficiency results in prolonged tail bleeding time, as well as protection in models of thrombosis and ischemic stroke[38].

1.5.2 Cell division control protein 42 homolog (Cdc42)

Cdc42 is a member of the Cdc42 subclass including Cdc42, RhoJ (TCL), RhoU (Wrch1), RhoV (Chp/Wrch2) and RhoQ (TC10)[36]. Cdc42 has a molecular weight of 21 kDa and was shown to be involved in filopodia formation and exocytosis. Constitutive Cdc42 null knockout mice do not survive early stages of embryonic development[39]. Conditional gene knockout for Cdc42 in platelets and MKs in mice results in a mild thrombocytopenia, which is thought to be caused by a pronounced decrease in platelet lifetime, together with a proplatelet formation defect. Furthermore, tail bleeding times of $Cdc42^{-/-}$ mice are prolonged while thrombus-formation is enhanced. Interestingly, filopodia formation of these mice is not altered and exocytosis is markedly increased[40].

1.6 Cell lines

1.6.1 K562 cell line

K562 cells are of the erythroleukemia type and were first described and established in 1975[41]. This cell line is derived from a chronic myelogenous leukemia patient in blast crisis. K562 cells can develop characteristics similar to

early-stage erythrocytes, granulocytes and monocytes[42]. Moreover, by inducing K562 cells with phorbol 12-myristate 13-acetate (PMA)[43] they differentiate into MK-like cells. While the differentiation process cannot be directly compared to normal stages of hematopoietic differentiation, K562 cells serve as a model system to study megakaryopoiesis.

1.6.2 Meg01 cell line

The Meg01 cell line is a human megakaryoblastic cell line first described and established in 1985[44]. It was obtained from the BM of a patient in blast crisis of Philadeplphia (Ph1) chromosome-positive chronic myelogenous leukemia. Meg01 cells express platelet GPIIb/IIIa and, upon maturation, also GPIb, thus providing a useful model system for the study of megakaryopoiesis and protein coupled biosynthetic mechanisms specific for megakaryocytic lineage.

1.7 Aim of the study

Polarization and podosome formation in MKs are thought to be crucial steps for PPF and release of platelets into the vascular system. It is hypothesized that these complex processes are co-regulated by Rho GTPase proteins like RhoA and Cdc42. However, the exact mechanisms by which different Rho GTPases regulate MK maturation, polarization and podosome formation remain incompletely understood.

In this thesis, these processes were investigated using MKs from genetically modified mice (with MK/platelet-specific conditional RhoA- and Cdc42-deficiency, respectively), as well as the human derived megakaryocytic cell lines Meg01 and K562.

Furthermore, signaling molecules and pathways for podosome formation were examined using pharmacological approaches (Src-kinase- and spleen tyrosine kinase (Syk)-inhibitors), as well as MKs from mice with conditional Syk- or GPVI-deficiency.

2 MATERIALS AND METHODS

2.1 Materials

2.1.1 Chemicals and reagents

Reagent	**Company**
Acetic acid	Carl Roth (Karlsruhe, Germany)
Agarose, low melting	Euromedex (France)
Ammonium peroxodisulphate (APS)	Carl Roth (Karlsruhe, Germany)
Bovine serum albumin (BSA)	AppliChem (Darmstadt, Germany)
Dynal Mouse T cell negative Isolation kit	Invitrogen (Carlsbad, CA, USA)
ECL solution	GE Healthcare (Freiburg, Germany)
Ethanol	Carl Roth (Karlsruhe, Germany)
Fat-free dry milk	AppliChem (Darmstadt, Germany)
Fibrillar type I collagen (Horm)	Nycomed (Munich, Germany)
Fluoresceine-5-isothiocyanate (FITC)	Molecular Probes (Karlsruhe, Germany)
Fluoroshield	Sigma-Aldrich (St. Louis, MO, USA)
Fluoroshield + DAPI	Sigma-Aldrich (St. Louis, MO, USA)
Fibrinogen from human plasma, Alexa Fluor® 488 Conjugat	Invitrogen (Carlsbad, CA, USA)
Fibrinogen	Sigma-Aldrich (St. Louis, MO, USA)
Fibronectin (human)	Sigma-Aldrich (St. Louis, MO, USA)
Fibronectin (murine)	Sigma-Aldrich (St. Louis, MO, USA)
GM6001	Merck Milipore (Billerica, MA, USA)
Igepal CA-630	Sigma-Aldrich (St. Louis, MO, USA)
Isopropanol	Carl Roth (Karlsruhe, Germany)
6x Loading Dye Solution	Fermentas (St. Leon-Rot, Germany)
Methanol	Carl Roth (Karlsruhe, Germany)
NH_4OH (10%)	AppliChem (Darmstadt, Germany)
NP-40	Sigma-Aldrich (St. Louis, MO, USA)
PageRuler Prestained Protein Ladder	Fermentas (St. Leon-Rot, Germany)

Paraformaldehyde (PFA)	Carl Roth (Karlsruhe, Germany)
Phalloidin-atto647N	Sigma-Aldrich (St. Louis, MO, USA)
PMSF	Merck Milipore (Billerica, MA, USA)
PP2	Merck Milipore (Billerica, MA, USA)
PP3	Merck Milipore (Billerica, MA, USA)
Protease-Inhibitor cocktail tabs	Roche Diagnostics (Mannheim, Germany)
Phorbol 12-myristate 13-acetate (PMA)	Sigma-Aldrich (St. Louis, MO, USA)
R406	Invivogen (Toulouse, France)
SDF1-α	Sigma-Aldrich (St. Louis, MO, USA)
TEMED	Carl Roth (Karlsruhe, Germany)
Triton X-100	Applichem (Darmstadt, Germany)
Tween 20	Carl Roth (Karlsruhe, Germany)
Vanadate	Sigma-Aldrich (St. Louis, MO, USA)

2.1.2 Cell culture materials

BSA, low endotoxin	PAA Laboratories (Cölbe, Germany)
D-PBS	Gibco (Karlsruhe, Germany)
Foetal Bovine Serum (FCS)	Gibco (Karlsruhe, Germany)
IMDM + GlutaMAX-I	Gibco (Karlsruhe, Germany)
Penicillin-Streptomycin	Gibco (Karlsruhe, Germany)
RPMI	Gibco (Karlsruhe, Germany)
Stem Cell Factor (SCF)	Invitrogen (Carlsbad, CA, USA)
Stempro®-34 serum-free medium	Gibco (Karlsruhe, Germany)
Thrombopoietin (TPO)	Invitrogen (Carlsbad, CA, USA)

2.1.3 Antibodies

2.1.3.1 Purchased primary and secondary antibodies

Anti-collagene-IV	Milipore (Billerica, USA)
Anti-GAPDH	Sigma-Aldrich (St. Louis, MO, USA)
Anti-p-ASAP1	Biomol (Hamburg, Germany)
Anti-RhoA	Cytoskeleton (Denver, CO, USA)
Anti-Tks5	Proteintech (Chicago, USA)
Anti-α-tubulin Alexa 488	Invitrogen (Carlsbad, CA, USA)
Anti-Wasp	Cell Signaling (Cambridge, UK)
Anti-Wasp	Santa Cruz Biotech. (Dallas, TX, USA)
CD11b antibody	BD Biosciences (Franklin Lakes, USA)
CD235a-FITC antibody	BD Biosciences (Franklin Lakes, USA)
CD3 antibody	BD Biosciences (Franklin Lakes, USA)
CD42b-FITC antibody	BD Biosciences (Franklin Lakes, USA)
CD45R/B220 antibody	BD Biosciences (Franklin Lakes, USA)
CD61-FITC antibody	BD Biosciences (Franklin Lakes, USA)
Chicken anti-goat Alexa Fluor 647	Invitrogen (Carlsbad, CA, USA)
Chicken anti-goat Alexa 488	Invitrogen (Carlsbad, CA, USA)
Cy3 antibody	Jackson IR (West Grove, PA, USA)
Polyclonal rabbit-anti-mouse IgG HRP	Dako (Glostrup, Denmark)
Polyclonal goat-anti-rabbit IgG HRP	Dako (Glostrup, Denmark)
Ly-6G/C antibody	BD Biosciences (Franklin Lakes, USA)
Ter-119 antibody	BD Biosciences (Franklin Lakes, USA)

2.1.4 Mice

8-to-12 week old mice of both sexes were used in experiments. Animal studies were approved by the district government of Lower Frankonia (Bezirksregierung Unterfranken).

RhoA[fl/fl 45], *Cdc42*[fl/fl 46] and *Syk*[fl/fl 47] mice were intercrossed with mice carrying the platelet factor 4 (Pf4)-Cre transgene (Pf4-Cre^{+/-}) to generate animals lacking Syk, RhoA or Cdc42 specifically in MKs and platelets. *Gp6*[-/- 48] mice were generated in our laboratory.

2.1.5 Buffers

If not declared otherwise, all buffers were prepared and diluted using *aqua ad iniectabilia* (DeltaSelect, Pfullingen, Germany) or double-distilled water (ddH2O).

ACK-Buffer, pH 7.2-7.4

NH_4CL	8.29 g/l
$KHCO_3$	1 g/l
NaEDTA	37.2 mg/l

Ammonium-hydroxide-solution

NH_4OH	0.2 mM

Blocking solution for immunoblotting

BSA or fat-free dry milk 5% in TBS-T

Buffer 1

PBS	main component
BSA low endotoxin	1 g/l
EDTA	4 mM

Carbonate Buffer

CO_3^{2-}	0.1 M

Citrate buffer (ph 5.4)

    Citric acid ($C_6H_8O_7$)   0.1 M

Laemmli buffer for SDS-PAGE

    TRIS   40 mM

    Glycine   0.95 M

    SDS   0.5%

Platelet lysis buffer

    PMSF 1mM   0,5%

    Protease inhibitor Cocktail   2%

    Natriumorthivanadate   2%

MK medium 1

    IMDM   main component

    FCS   10%

    Penicillin-Streptomycin   1%

    Glutamin

      1%

MK medium 2

    Stempro®-34 serum-free medium   500 ml

    StemPro®-34 Nutrient Supplement   13 ml

    Penicillin-Streptomycin   1%

    Glutamin   1%

Natrium-hydroxide-solution

    NaOH   3M

PHEM buffer

PIPES	100 mM
HEPES	5.25 mM
EGTA	10 mM
$MgCl_2$	20 mM

Phosphate buffered saline (PBS), pH 7.14

NaCl	137 mM
KCl	2.7 mM
KH_2PO_4	1.5 mM
Na_2HPO_4	8 mM

RPMI medium

RPMI IMDM	main component
FCS	10%
Penicillin-Streptomycin	1%
Glutamin	1%

SDS sample buffer, 4x

β-Mercaptoethanol	10%
TRIS buffer (1.25 M), pH 6.8	10%
Glycerine	20%
SDS	4%
Bromophenolblue	0.02%

Separating gel buffer

TRIS/HCl (pH 8.8)	1.5 M

Serum Free RPMI

RPMI	main component
Penicillin-Streptomycin	1%
Glutamin	1%

Stacking gel buffer

    TRIS/HCl (pH 6.8)   0.5 M

Mild stripping buffer, pH 2

    SDS   1%

    Glycine   25 mM

Tris-buffered saline (TBS), pH 7.3

    NaCl   137 nM

    Tris/HCl   20 mM

Washing buffer for Western blot (TBS-T)

    TBS   main component

    Tween 20   0.1% in TBS

2.2 Methods

2.2.1 MK culture

2.2.1.1 *In vitro* differentiation of BM-derived MKs via lineage depletion

Adult mice were sacrificed by cervical dislocation under isoflurane anesthesia. Femora of mice were isolated and the BM was flushed out using 22G needles, a 1 ml syringe and 2 ml MK Medium 1. In the next step, these samples were homogenized by resuspending them 10 times and counted using a Neubauer chamber. Primary erythrocyte removal was achieved via erythrocyte-lysis. For this, the cells were transferred into conical centrifugation tubes (Greiner centrifuge tube, Greiner Bio-One, Kremsmünster, Austria) of 15 ml volume, centrifuged 7 mins at 1200 rpm, RT, and resuspended in 1 ml ACK-buffer per sample. After a 5 min incubation time 1 ml PBS was added to stop the reaction and the cells were again centrifuged for 7 mins at 1200 rpm, RT. MKs and HSCs were further purified by negative selection using the following antibodies: CD45R/B220 (specific for leukocytes), TER-119 (specific for erythrocytes), CD3

(specific for T-cells), Ly-6G/C (specific for neutrophils) and CD11b (specific for leukocytes). To achieve purification, the pellet was resuspended in 100 µl ice cold buffer 1 per $1x10^7$ cells. 20 µl FCS (HI) and 0.5 µg of each antibody per $1*10^7$ cells were added and mixed well followed by incubation on ice for 20 mins. Samples were then washed using 2 ml of buffer 1 per $1x10^7$ cells and centrifuged 8 mins at 300 g (4°C). In the following, the pellet was resuspended in a mixture of 800 µl buffer 1 and 200 µl pre-washed magnetic beads (Dynabeads® FlowComp™ Human CD4 Kit, Life Technologies, Carlsbad, CA, USA) per $1x10^7$ cells and incubated 15 min with gentle tilting and rotation at RT. 1 ml of buffer 1 per $1x10^7$ cells was added and the bead-bound cells were gently resuspended. After placing the tubes in magnetic racks for 4 mins, the supernatant was collected and transferred into a new tube. The cells were again counted and centrifuged 5 mins at 200 g, 4°C. The cells were cultured in 12-well plates (Falcon® Multiwell Plates for Cell Culture, BD Falcon, Franklin Lakes, USA) at a concentration of $0.5x10^6$ cells/ml 'MK medium 1' supplemented with 50 ng/ml thrombopoietin (TPO) for 3 days at 37°C, 5% CO_2 for further analysis. Samples were enriched for MKs by layering the cells on 1.5 - 3.0% BSA/PBS single-step gradients in 15 ml canonical centrifugation tubes and allowed to settle down for 30 mins. After withdrawing the upper part of the suspension except for 1 ml, the enriched MKs were washed with 2 ml MK Medium 1, centrifuged down again and resuspended in 250 µl MK Medium 1 and ready for further experiments

2.2.1.2 *In vitro* differentiation of BM-derived MKs using the MK enrichment method

Adult mice were sacrificed by cervical dislocation under isoflurane anesthesia. Femora of mice were isolated and the BM was flushed out using a 22G needle, a 1 ml syringe and 2 ml 'MK medium 2'. In order to prepare single cell suspensions, the solutions were pipetted up and down 5-7 times using first 1 ml tips by pipetting, followed by 18 and 22 gauge needles. Finally 25 gauge needles were used to pipet the solutions 2 times up and down. To ensure the removal of bone and other solid tissue parts, the probes were passed through cell strainers (Easy strainer 70 µm, Greiner Bio-One, Kremsmünster, Austria). The cell

strainers were washed with 1 ml medium, respectively, and then spun down for 5 mins at 200 g, RT in a canonical centrifugation tubes. Finally, the cell pellets were resuspended in 5 ml 'MK medium 2' supplemented with 50 ng/ml stem cell factor (SCF) and cultured for 2 days in 2 wells of a 6 well plate at 37°C, 5% CO_2.

After the first culture period, the cells were spun down again for 5 mins at 200 g, RT. The pellets were resuspended in 5 ml fresh 'MK medium 2' supplemented with 50 ng/ml SCF and 50 ng/ml TPO and then cultured for 2 more days in 2 wells of a new 6 well plate at 37°C, 5% CO_2.

Cut-tip pipet tips were used from now on to minimize the influence of shear-force for MK development.

When the second culture period was finished, medium was exchanged again as described previously, this time supplemented solely with 50 ng/ml TPO and cultured for 1 more day in 2 wells of a new 6 well plate at 37°C, 5% CO_2.

After the third culture period, cells were again spun down for 5 mins at 200 g, RT and resuspended in 1 ml 'MK medium 2'. Samples were enriched for MKs by using a 1.5 - 3.0% BSA/PBS gradient as described above. Enriched MKs were now re-cultured in 5 ml medium without any further supplements in 2 wells of a new 6 well plate at 37°C, 5% CO_2 for one day.

Analysis was performed at day 6, when the fourth culture period was completed.

2.2.1.3 K562 cell differentiation

$2x10^5$ K562 cells were cultured in a volume of 10 ml RPMI medium at 37°C, 5% CO_2 (day 0). On day 1 cells were supplemented with 100 ng/ml phorbol 12-myristate 13-acetate (PMA), inducing the differentiation towards MKs. From day 1 until day 4, cell numbers were determined by daily counting with the Neubauer chamber. The cells were resuspended once every day to prevent excessive cell clotting. Experiments were performed on day 4 of culture.

2.2.2 Cell analysis

2.2.2.1 MK lysates and Western Blot

For Western blot analysis samples were centrifuged for 5 mins at 200 g and then resuspended in Lysis buffer to a final concentration of 1×10^6 cells per 100 µl. After incubation for 30 min on ice and centrifugation at 14000 rpm for 5 min, the supernatant was mixed with 4x SDS sample buffer and boiled at 95°C for 5 min in order to achieve protein denaturation. In the following step, the samples were separated by loading 20 µl per lane onto a 10% or 12% polyacrylamide gel and run at 20-25 mA for 1.5 h. Samples were transferred onto a polyvinylidene difluoride (PVDF) membrane via semi-dry blotting at a current of 50 mA per gel. To avoid non-specific antibody binding, membranes were blocked in 50 ml blocking buffer (5% BSA or 5% fat-free milk dissolved in TBS-T buffer) for 1 h at RT. Membranes were incubated with 5 ml of the required blocking buffer supplemented with the appropriate primary antibody (5 µg/ml) over night at 4°C with gentle shaking. Next, the membranes were washed three times with TBS-T buffer for 10 min at RT under shaking conditions. Afterwards, they were incubated with corresponding horseradish peroxidase (HRP) - labeled secondary antibodies for 1 h at RT. After three washing steps, proteins were visualized by enhanced chemiluminescent substrate (ECL).

2.2.2.2 FACS analysis of differentiated K562-cells

In order to determine differentiation/maturation levels, 200 µl of the cell suspensions were incubated with 2 µl fluorescein-isothiocianate-conjugated (FITC) antibodies CD42b-FITC, CD61-FITC, and CD235-FITC which are specific for MK- and erythrocyte-binding (kindly provided by the research group of Professor Dr. Harald Schulze, Institut für Experimentelle Biomedizin, Universitätsklinikum Würzburg). Samples were incubated for 20 minutes at 4°C and the reaction was stopped by addition of 300 µl PBS. The probes were then analyzed on a FACSCalibur (BD Biosciences, Heidelberg, Germany).

2.2.2.3 Spreading of cells on ECM surfaces for analysis of polarization and podosome formation

Rectangular 24 x 60 mm glass coverslips (Roth, Karlsruhe, Germany) were coated with 150 µl/slide of fibrillar collagen I (50 µg/ml), fibrinogen (100 µg/ml) or fibronectin (10-100 µg/ml) and incubated over night at 4°C in dark humid chambers. After 3 washings steps with 350 µl PBS each, the slides were blocked with 200 µl culture medium for 1 h, 37°C, 5% CO_2. For the analysis of Meg01 cells on fibronectin, cells were starved for 1 h in RPMI medium without FCS. For all further cell analysis on other ECMs this step was not needed. Next, the cells were seeded and incubated for 3 h at 37°C, 5% CO_2. Adherent cells were fixed and permeabilized by adding 250 µl Phem buffer supplemented with PFA (4%) and NP-40 (1%) for 20 min, RT. After 3 more washing steps the slides were blocked by adding 200 µl BSA/PBS (3%) for 45 min at RT. In the following steps the cells were stained for immunofluorescence analysis by confocal microscopy. The samples were stained with phalloidin-Atto647N and/or with anti-α-tubulin Alexa 488 in dark humid chambers for 75 mins at 37°C and 5% CO_2. Occasionally, third antibody staining was performed. Afterwards, the samples were mounted to microscope glass slides (Thermo scientific, Waltham, MA, USA) using Fluoroshield™ with or without DAPI and stored at 4° until analysis. Imaging was performed using a Leica TCS SP5 confocal microscope (Leica Microsystems, microscopy platform of the Bioimaging Center, Rudolf Virchow Center für Experimentelle Biomedizin Würzburg).

2.2.2.4 Podosome formation and degradation of MKs on prelabeled fibrinogen

This assay was performed according to chapter 2.2.2.4 (Spreading of cells on ECM surfaces for analysis of polarization and podosome formation) with the difference that coverslips were coated with ´Fibrinogen from Human Plasma, Alexa Fluor® 488 Conjugate' (100 µl/ml). Cells were seeded in MK Medium containing SDF-1α, and antibody staining was solely performed for the F-actincytoskeleton.

2.2.2.5 Podosome formation and degradation of MKs on Peritoneal Basement Membrane (PBM)

Young mice (≤ 8 weeks) were sacrificed by cervical dislocation under isoflurane anesthesia. Peritoneum was removed and decellularized by transferring it to a cell crown (CellCrown™24, non-sterile, Scaffdex Oy, Finland) and incubating it in 50 ml NH_4OH (0.2 mM) with gentle tilting and rotation for 1h at RT. After transferring the samples into a 24 – Culture Multiwell Plate (Sigma Aldrich®, St. Louis, USA) followed by 3 washing steps with ice cold PBS (1.5 ml/membrane), MKs were seeded on top of the membranes and incubated for 3h at 37°C and 5% CO_2. Next, samples were fixed and permeabilized using 500 µl Phem buffer supplemented with PFA (4%) and Triton X-100 (0.1%) for 15 min at RT followed by 2 washing steps with PBS. In the following steps the samples were stained using a primary antibody against collagen IV and its corresponding secondary antibody, as well as phalloidin-Atto647N, followed by 2 washing steps, respectively. The samples were stored in PBS at 4°C.

For imaging, samples were removed from the cell crown and mounted onto glass slides using Fluoroshield with or without DAPI, coverslips and Parafilm® samples were then stored 1 h at 4°C until confocal imaging (Leica TCS SP5 confocal microscope (Leica Microsystems)).

2.2.2.6 Data analysis using 'Fiji', Excel, SigmaPlot and PowerPoint

Podosome number and size was measured semi-automated using 'Fiji' (open source project software developed by Johannes Schindelin, Albert Cardona, Mark Longair, Benjamin Schmid, and others). An already developed and tested counting macro[49] was used to analyze preselected and processed areas.

MK size was measured manually using 'Fiji'-measuring tools.

Data was collected and further analyzed using Excel (Microsoft).

Figures and Images were processed using SigmaPlot 13.0 (Systat Software GmbH) and PowerPoint (Microsoft).

3 RESULTS

3.1 MK Polarization

3.1.1 BM-derived MKs and Meg01 cells do not polarize on fibronectin while PMA-induced K562 cells show clear polarization patterns

After maturation and contact with BM sinusoid cells, MKs produce platelets by extending proplatelet protrusions into the sinusoid lumen. This occurs in a directed way. Thus, MKs must be able to polarize. Rho GTPases RhoA and Cdc42 are known as regulators of polarization and migration and were therefore analyzed in the following.
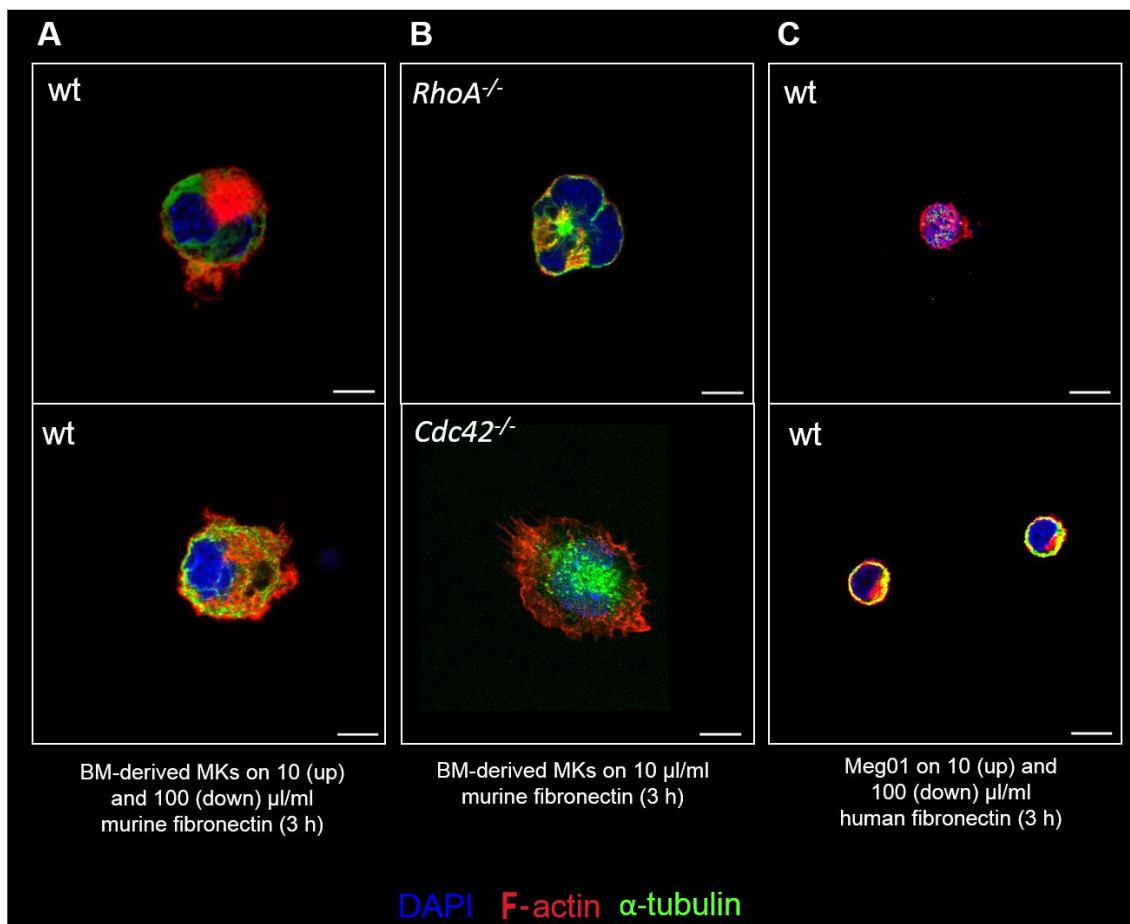

Figure 8: Analysis of BM-derived MKs and Meg01 cells on fibronectin.
WT (A), *RhoA-/-* and *Cdc42-/-* MKs (B) and Meg01 cells (C) were allowed to spread on fibronectin (here shown: 10 µg/ml and 100 µg/ml) coated glass coverslips, incubated for 3 h and then fixed and stained with DAPI (blue) and for F-actin (red) and α-tubulin (green). Images show an overlay of all three channels and are representative for ≥ 3 cells of ≥ 3 individuals. All images were acquired with a Leica TCS SP5 confocal microscope (Leica Microsystems) using a 63x objective. Scale bars represent 10 µm.

WT and *RhoA*^{-/-} or *Cdc42*^{-/-} BM-derived MKs were incubated on fibronectin-coated (10 µl/ml, 25 µl/ml, 50 µl/ml, 100 µl/ml) glass coverslips. All analyzed MKs displayed round morphology with a size from 20 up to 40 µm without major polarized F-actin or tubulin cytoskeleton structures, protrusions or membrane ruffling (Figure 8 A, B).

Cells from the megakaryoblastic cell line Meg01, analyzed under similar conditions, did not show any polarization patterns. Cellular morphology analysis revealed mainly round cells of a size from 10 µm to 20 µm (Figure 8 C).

In general, analyzed BM-derived MKs and Meg01 cells showed similar morphology on all different concentrations of fibronectin (not shown).

K562 cells were induced with phorbol 12-myristate 13-acetate (PMA) in order to induce differentiation in MK-like cells and thus lose their ability of logarithmic growth (confirmed in the following Chapters: 3.1.2.1 – 3.1.2.3). So they could be further used for basic studies on MK behaviour[50]. After seeding and incubating differentiated K562 cells on different concentrations of human derived fibronectin, polarization could be observed and evaluated via immunofluorescence imaging (Figure 9). Typical polarization patterns - long F-actin and tubulin rich cell protrusions – could be observed (Figure 9 B left), as well as so called membrane ruffles (Figure 9 B right), a characteristic feature of many actively migrating cells. The high F-actin concentrations in the area of the ruffling membranes are a strong indication for cell polarity. K562 cells without PMA treatment (Figure 9 A) lacked these features.
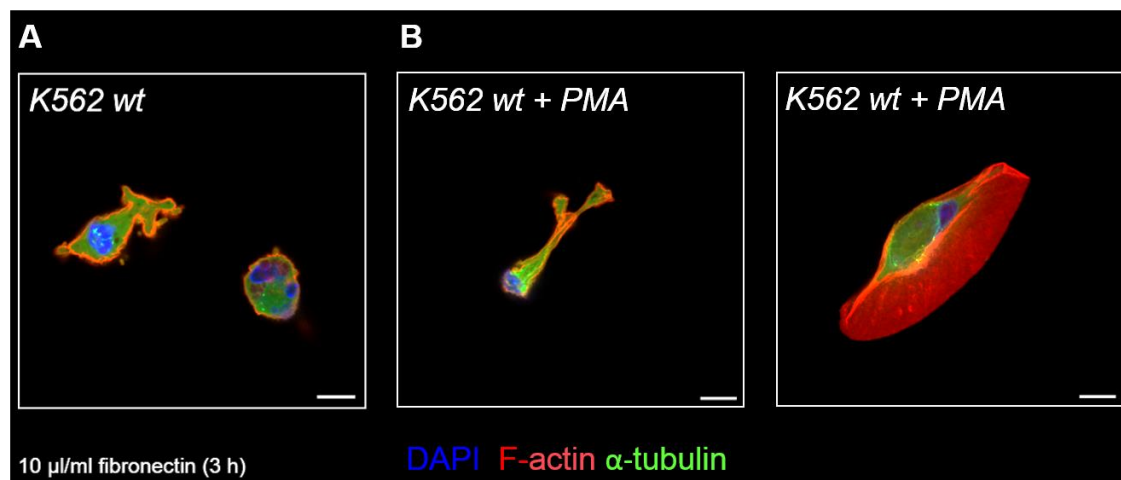
Figure 9: PMA-induced K562 cells polarize on fibronectin.
Control cells without PMA (A) and PMA induced cells (B) of the K562 cell line were allowed to spread on fibronectin-coated (10 µg/ml) glass coverslips, incubated for 3 h and then fixed and stained with DAPI (blue) and for F-actin (red) and α-tubulin (green). Representative images show an overlay of all three channels. All images were acquired with a Leica TCS SP5 confocal microscope (Leica Microsystems) using a 63x objective. Scale bars represent 10 µm.

3.1.2 Generation of RhoA$^{-/-}$ K562 cells using the CRISPR/Cas9 system

In order to analyze the influence of RhoA on polarization, *RhoA*$^{-/-}$ K562 cell clones (named A8 and H12) were generated by Simon Stritt using the CRISPR(clustered regularly interspaced short palindromic repeats)/Cas9-system. The CRISPR /Cas9-system is a molecular biological tool, which can be used for targeted genome editing[51]. It is originally derived from prokaryotic cells, which use this technology as a part of their acquired immunity, enabling the cell resistance to pathological genetic elements such as plasmids[52]. Using a bacteria-derived vector-system for cell transfection, individually engineered RNA-guided nucleases (e.g. Cas9) can be generated (Figure 10 A). These nucleases are used to perform double-strand breaks in defined genomic sequences in order to initiate targeted deletions, insertions or modifications of desired exons through non-homologous end-joining (NHEJ) or homology-directed repair (HDR) (Figure 10 B). Compared to other genome-editing tools, this system is easy and fast. Multiple different cell types have already been genetically edited successfully[51].
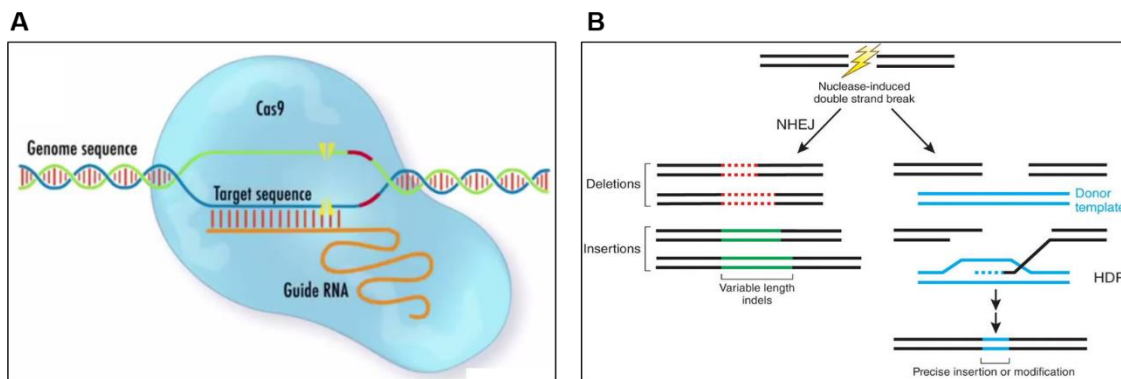
Figure 10: The CRISPR-Cas-System.
(A) Genome sequences are precisely selected by customized RNA-guided nucleases (here Cas 9) which are able to recognize exact target sequences. After recognition through the guide RNA, double strand breaks are initiated by the nuclease. (B) RNA-guided nucleases induced double strand breaks, which can be repaired in two ways. Non-homologous end-joining (NHEJ) results in imprecise insertion mutations of variable length or deletion mutations. Homology-directed repair (HDR), however, uses single-stranded or double stranded DNA donor templates to produce precise point mutations, insertions and modifications. <u>Abbreviations:</u> NHEJ = non-homologous end-joining; HDR = homology-directed repair

(A) Modified from the video: "Quick learning of CRISPR/Cas9"; internet website of OriGene Technologies Inc.[53]
(B) Taken from: Sander JD et al.; Nat Biotechnol.; 2014[51]

Successful RhoA-depletion of the generated cell clones was confirmed by Western blot analysis of lysates of WT K562 cells and clones A8 and H12 using WT and *RhoA*^{-/-} platelet lysates as a positive control (Figure 11 A). In all Western blot assays Glycerinaldehyde-3-phosphat-Dehydrogenase (GAPDH) was used as a loading control.

Curiously, further Western blot analysis revealed the absence of RhoA not only in genetically modified K562 cell clones with or without PMA-treatment, but also in WT PMA-treated K562 cells (Figure 11 B).
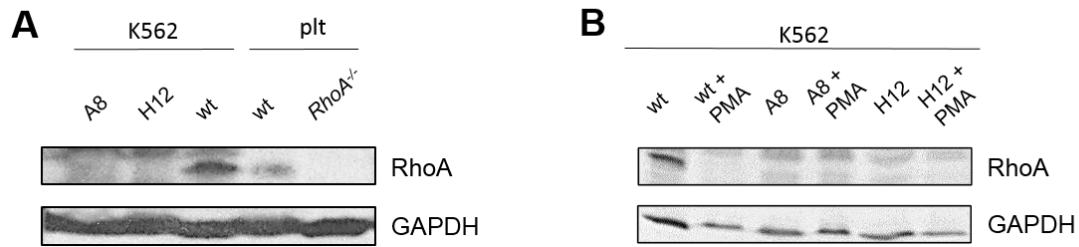
Figure 11: RhoA expression is downregulated in cell clones A8 and H12, as well as in PMA stimulated K562 cells.
(A) Western blot analysis of RhoA expression in WT K562 cells and WT platelets versus *RhoA^-/-^* K562 clones (A8 and H12) and *RhoA^-/-^* platelets. (B) RhoA expression of WT K562 and *RhoA^-/-^* K562 clones was analyzed against their PMA-incubated counterparts. GAPDH expression was used as loading control in both experiments.

3.1.2.1 Analysis of the effect of differentiation status and RhoA depletion on the proliferation of K562 cells

In order to determine cell proliferation of the different K562 cell lines and clones, WT cells and *RhoA^-/-^* cell clones A8 and H12 were seeded at day 0 at a concentration of 0.2×10^5 cells/ml. The three cell samples were cultured with and without PMA for 4 days.

K562 control cells proliferated until day 4 to a number of 1.60×10^5 cells/ml. The growth potential of untreated *RhoA^-/-^* K562 cell clones was slightly lower: clone A8 1.45×10^5 cells/ml, clone H12 1.30×10^5 cells/ml (Figure 12).

The proliferation of the cells was strongly reduced upon PMA treatment. Under these conditions, WT K562 cells displayed a final concentration of 0.40×10^5 cells/ml, *RhoA^-/-^* K562 clone A8 0.20×10^5 cells/ml and clone H12 0.45×10^5 cells/ml at day 4 (Figure 12).
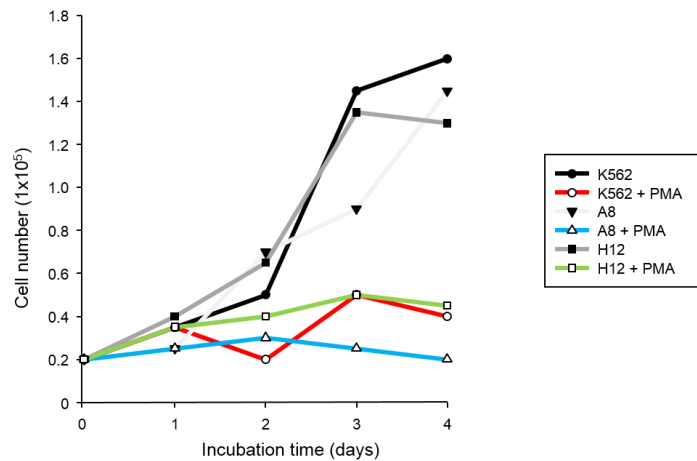
Figure 12: RhoA-deficient K562 cells grow normally while the proliferation of PMA-treated cells is strongly reduced.
Proliferation of WT and *RhoA-/-* K562 cells (untreated and PMA-treated) over time was determined using a Neubauer chamber. Results are representative for 3 experiments.

3.1.2.2 Morphological analysis

During the time of cultivation, the samples were analyzed for their morphology by light microscopy.

Control K562 cells displayed strong growth, homogenous size and a round appearance. Strong cell clustering had to be reduced by resuspending the suspension.

RhoA-/- control K562 cells showed a slight decrease in proliferation, and strongly heterogeneous morphology. Some cells appeared increased in size and displayed rough border zones.

PMA treated K562 WT cells displayed a strong decrease in cell number and morphological analysis revealed heterogeneous cell shape and rough margins. PMA treated *RhoA-/-* K562 cells displayed an even stronger decrease in cell number and morphological alterations were more pronounced.

3.1.2.3 Levels of differentiation

FITC-labeled anti-CD61 and anti-CD42b-labeled antibodies were used to quantify MK receptors GPIIIa (integrin β3) and GPIbα. Anti-CD235a-FITC labeled antibody was used to detect the erythrocyte receptor Glycoprotein A (GYPA). GPIIIa is part of the transmembrane receptor integrin αIIbβ3 on the surface of platelets and crucial for fibrinogen binding and aggregation. GPIbα is part of the

GPIb-IX-V receptor complex which is important for von Willebrand factor (VWF) dependent platelet adhesion after vascular injury, as well as platelet activation, thrombosis and hemostasis. Levels of differentiation were determined by comparing the fluorescence signals of PMA treated samples to control samples analyzed by flow cytometry. In addition, intensities of the forward scatter signal (FSC) (for the analysis of cell size) and the side scatter signal (SSC) (for the analysis of cell granularity) of all samples were evaluated.

Very dense population characteristics in flow-cytometry dot plots regarding size and granularity are typical for untreated K562 cells (Figure 13 A left). PMA treated K562 cells displayed higher granularity (Figure 13 A right, Figure 16 B), however, mean cell size remained unaltered (Figure 13 A right, Figure 16 A).

RhoA$^{-/-}$ K562 cell clones A8 and H12 showed moderately altered characteristics: untreated populations already displayed cells with a heterogeneous granularity (Figure 14 A left, Figure 15 A left, Figure 16 B) compared to WT K562 cells. This spread in granularity was even stronger upon treatment with PMA (Figure 14 A right, Figure 15 A right, Figure 16 B). In contrast, cell size was unaltered compared to WT K562 cells (Figure 16 A). CD42b-expression in K562 WT cells was low, as expected. A strong increase in CD42b-positive cells was detected, when differentiation towards MKs was induced with PMA (Figure 13 B, Figure 16 C). *RhoA*$^{-/-}$ K562 cell clones A8 and H12 already displayed a higher basic level of CD42b-positive cells and showed an increased receptor expression after PMA stimulation (Figure 14 B, Figure 15 B, Figure 16 C). Findings for CD61-positive cells were similar to CD42b-positive cells (Figure 13 C, Figure 14 C, Figure 15 C, Figure 16 D). The characteristic erythrocyte marker CD235a was expressed at a relatively high level in untreated WT K562 cells and not significantly reduced after PMA treatment (Figure 13 D, Figure 16 E). *RhoA*$^{-/-}$ K562 cell populations A8 and H12 displayed higher basal numbers of CD235a-positive cells that were strongly decreased after PMA treatment (Figure 14 D, Figure 15 D, Figure 16 E). Thus, *RhoA*$^{-/-}$ K562 cells lose erythrocyte characteristics and gain MK characteristics when treated with PMA.
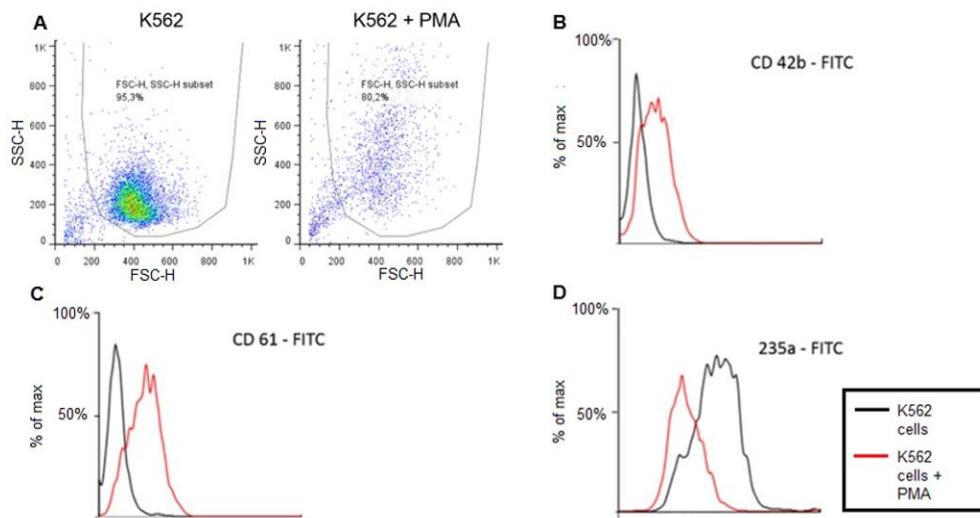
Figure 13: K562 WT cells gain MK characteristics and loose erythrocyte characteristics when treated with PMA.

K562 WT cells (A-D) without and with PMA treatment were analyzed by flow cytometry. (A) shows dot plot analysis of population distribution with regards to size (forward scatter (FSC)) and granularity (side scatter (SSC)). (B-D) show histograms for visualization of the shift of untreated (black lines) and PMA treated (red lines) cell populations with regard to surface-protein expression. Results are representative of 3 experiments.

Figure 14: *RhoA*-/- K562 cell clones gain MK characteristics and loose erythrocyte characteristics when treated with PMA.

RhoA-/- K562 cells (clone A8) without and with PMA treatment were analyzed by flow cytometry. (A) shows dot plot analysis of population distribution with regards to size (forward scatter (FSC)) and granularity (side scatter (SSC)). (B-D) show histograms for visualization of the shift of untreated (black lines) and PMA treated (red lines) cell populations with regard to surface-protein expression. Results are representative of 3 experiments.
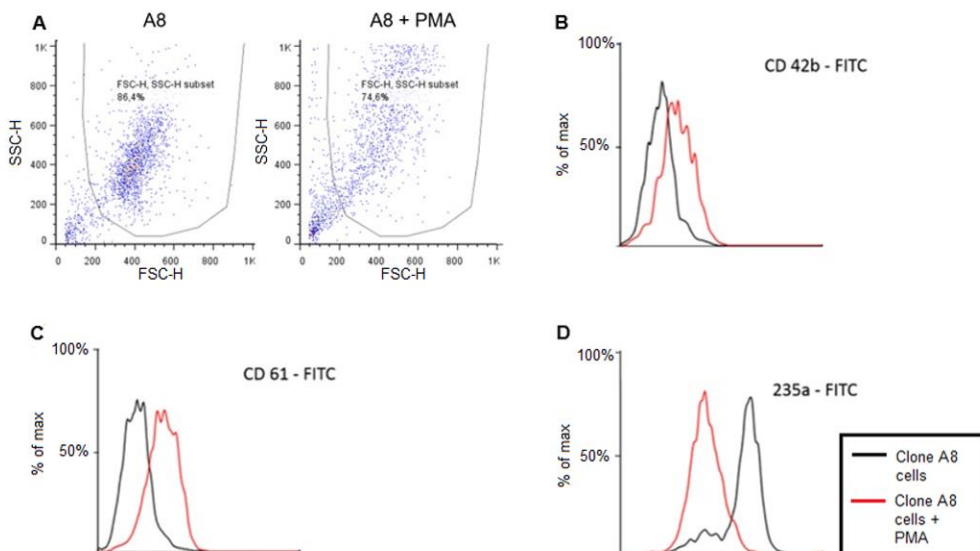
Figure 15: *RhoA^{-/-}* K562 cell clones gain MK characteristics and loose erythrocyte characteristics when treated with PMA.

RhoA^{-/-} K562 cells (clone H12) without and with PMA treatment were analyzed by flow cytometry. (A) shows dot plot analysis of population distribution with regards to size (forward scatter (FSC)) and granularity (side scatter (SSC)). (B-D) show histograms for visualization of the shift of untreated (black lines) and PMA treated (red lines) cell populations with regard to surface-protein expression. Results are representative of 3 experiments.
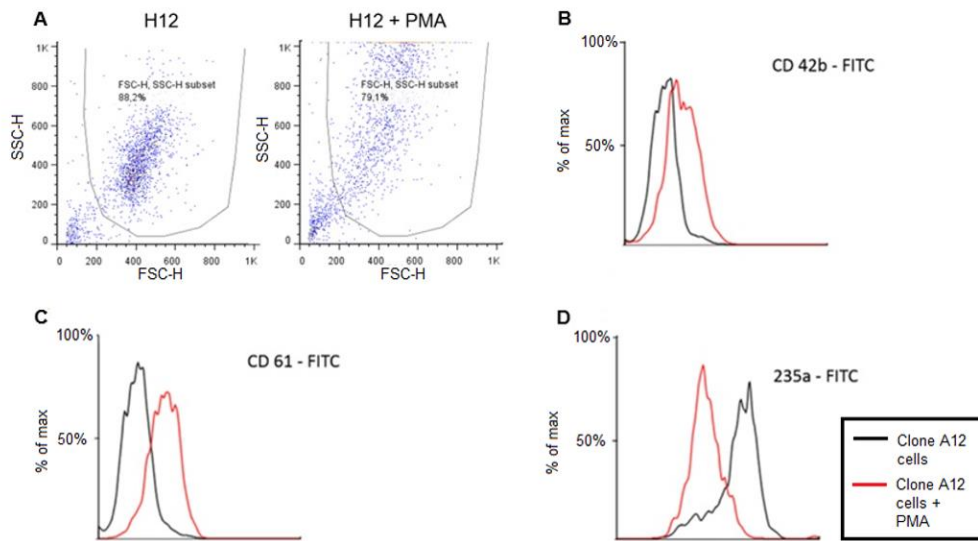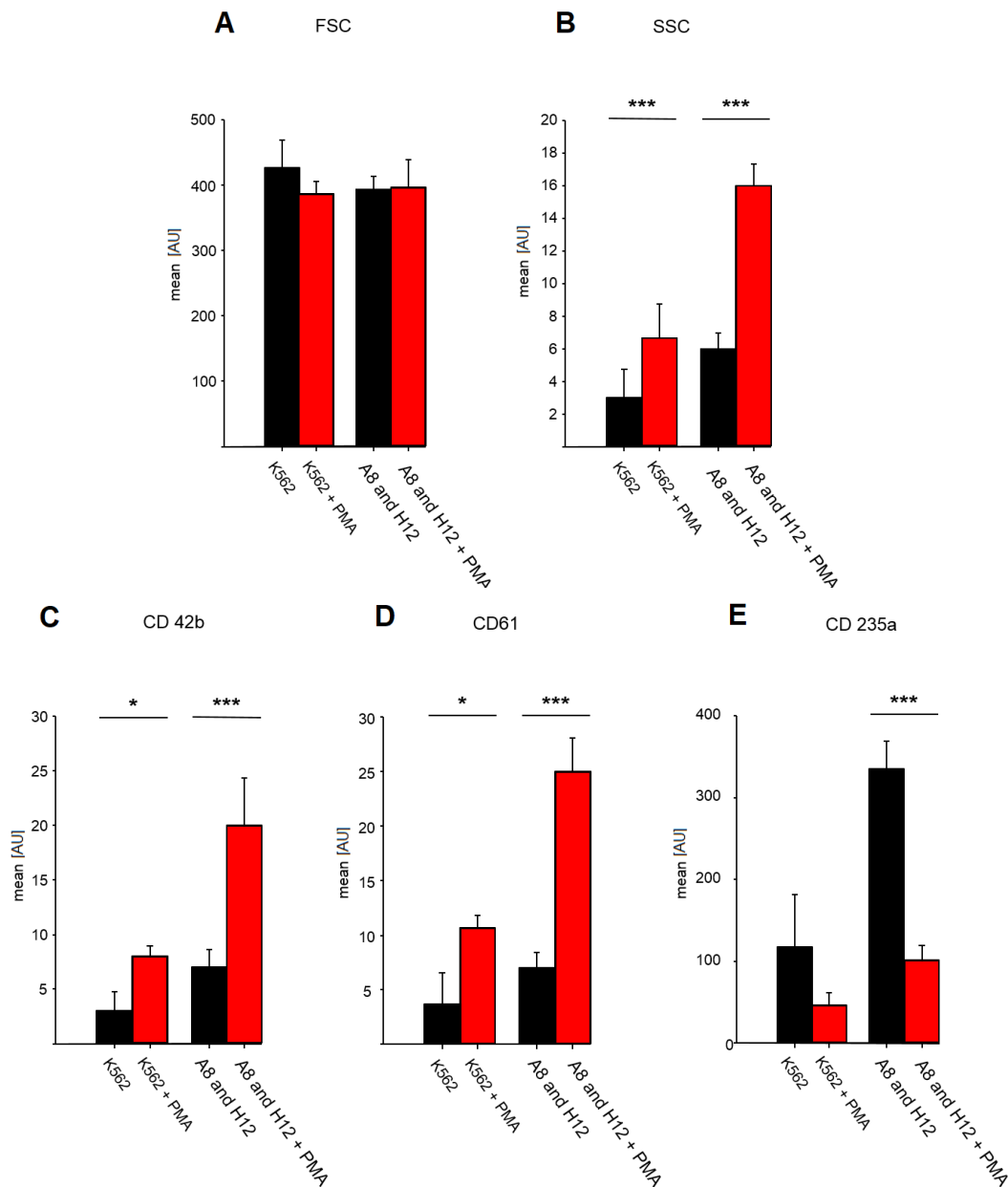
Figure 16: Bar graph quantification of untreated and PMA treated WT and *RhoA-/-* K562 cells.
(A) and (B) show bar graph analysis of size and granularity. MK surface-protein expression is presented in (C) and (D) (CD61 and CD42b), erythrocyte surface protein expression in (E) (CD235a). K562 WT cells (black bar graph left) are compared to PMA treated K562 WT cells (red bar graph left) and *RhoA-/-* K562 cells (black bar graph right) compared to PMA-treated *RhoA-/-* K562 cells (red bar graph right). Results are representative of 3 experiments. Data is presented as mean ± SD of n ≥ 3 cell populations. *P<0.05, **P<0.01, ***P<0.001 (Student's t-test).

3.1.3 *RhoA⁻/⁻* K562 cell clones display altered polarization upon adhesion on fibronectin

Spreading of untreated, PMA-treated K562 WT (Figure 9) as well as untreated and PMA-treated K562 *RhoA⁻/⁻* cell clones A8 and H12 (Figure 17) on human fibronectin (10 µl/ml and 100 µl/ml) was analyzed by confocal microscopy. Preliminary results revealed typical membrane ruffles (Figure 17 A) and protrusions (Figure 17 B) in all cells. However, only PMA-induced *RhoA⁻/⁻* K562 cells exhibited both multiple membrane ruffles and multiple polarization protrusions (Figure 17 B,C). In contrast to K562 WT cells, polarization patterns were also found in non-PMA-induced *RhoA⁻/⁻* cells (Figure 17 D).
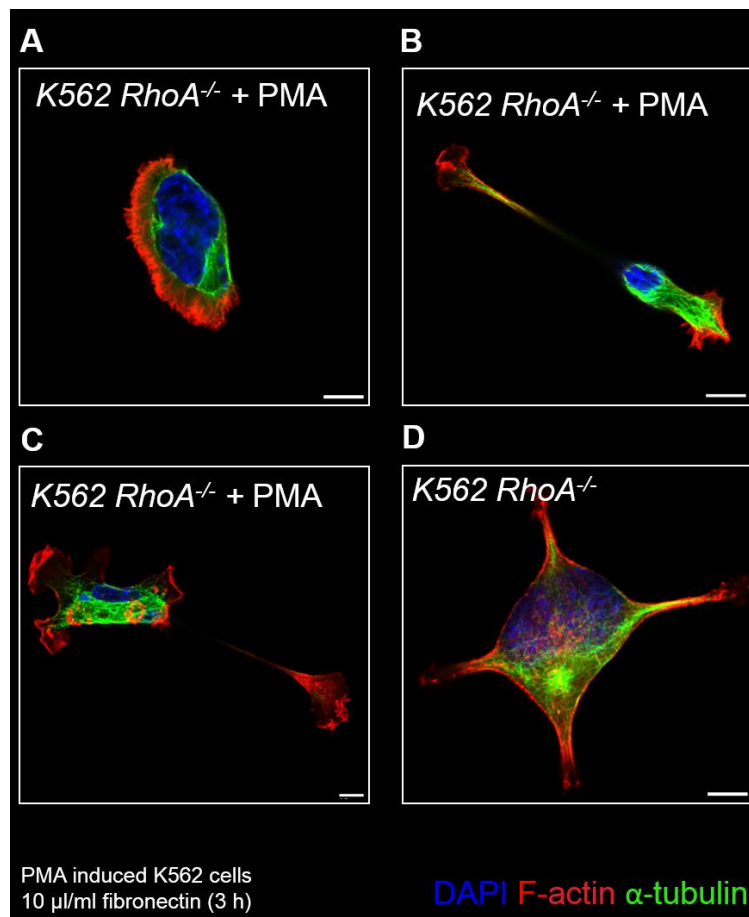

Figure 17: K562 CRISPR *RhoA⁻/⁻* cell clones display altered polarization patterns upon adhesion on fibronectin.
PMA induced (A-C) and untreated (D), *RhoA⁻/⁻* K562 were allowed to spread on fibronectin-coated (10 µg/ml) glass coverslips, incubated for 3 h and then fixed and stained with DAPI (blue) and for F-actin (red) and α-tubulin (green). Representative images show an overlay of the three channels. All images were acquired with a Leica TCS SP5 confocal microscope (Leica Microsystems) using a 63x objective. Scale bars represent 10 µm.

As shown by Western blot analysis, RhoA expression was downregulated in WT K562 cells treated with PMA (Figure 11). This observation raises the interesting question whether decreased RhoA expression directly contributed the differentiation towards an MK-like phenotype and to the altered polarization patterns of PMA-treated compared to untreated WT K562 cells.

3.2 Functional analysis of podosome formation in MKs

BM-derived MKs of WT mice build up podosomal structures in response to contact with certain BM-associated ECM proteins, such as collagen I and fibrinogen. Upon immunofluorescence staining, podosomes appeared as dotted F-actin-rich structures close to the substrate in adherent MKs. To prove that these labeled structures are indeed podosomes, colocalization of F-actin and the podosome marker p-ASAP1[54] was investigated. On collagen I, as well as on fibrinogen-coated glass coverslips (Figure 18 A, B) F-actin and p-ASAP1 staining colocalized (appearing as white dots in the overlay) and thus confirmed these structures as podosomes.
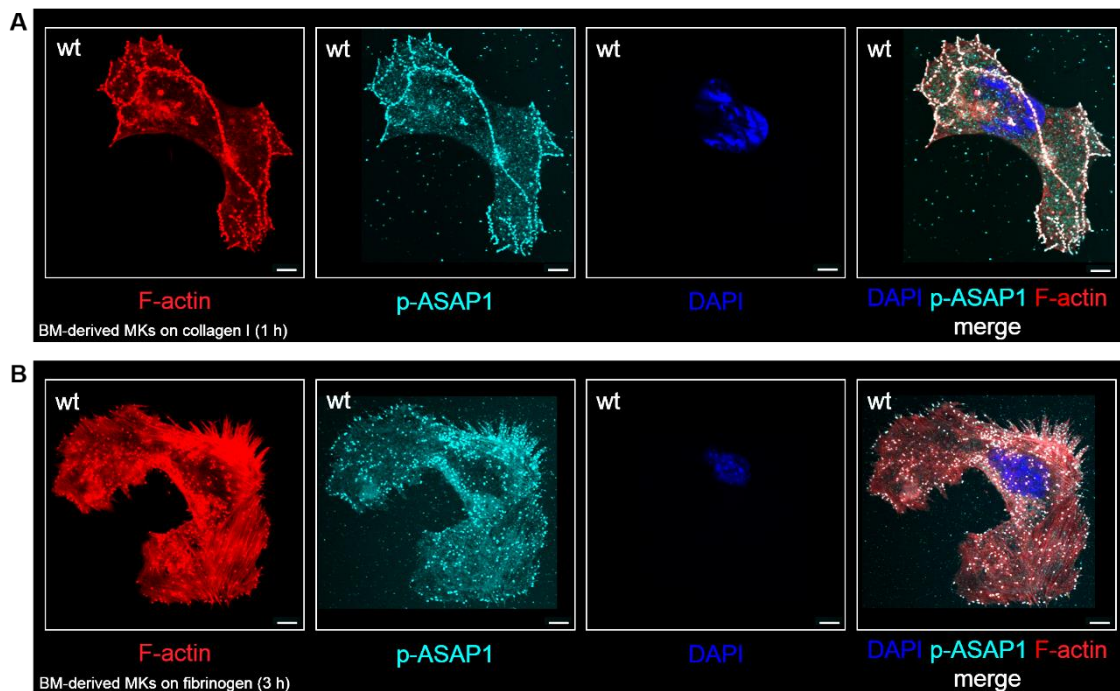
Figure 18: MKs assemble podosomes on fibrillar collagen I (A) and fibrinogen (B).
BM-derived MKs were allowed to spread on fibrillar collagen I- (50 µg/ml) or fibrinogen-coated (100 µg/ml) glass coverslips, incubated for 1 h (fibrillar collagen I) or 3 h (fibrinogen) and then fixed and stained with DAPI (blue) and for F-actin (red), p-ASAP1 (cyan). Colocalisation of F-actin and p-ASAP1 appears white (right). All images were acquired with a Leica TCS SP5 confocal microscope (Leica Microsystems) using a 63x objective. Scale bars represent 10 µm.

3.2.1 *RhoA*^{-/-} and *Cdc42*^{-/-} MKs display unaltered or slightly decreased capability of podosome formation on different ECM components

RhoA and Cdc42 are important players in the regulation of the cytoskeleton. Therefore, the loss of either of them may lead to alterations of intracellular F-actin and tubulin polymerization and rearrangement. To investigate this, BM-derived WT MKs, as well as *RhoA*^{-/-} and *Cdc42*^{-/-} MKs were allowed to spread on fibrillar collagen I- (Figure 19) or fibrinogen-coated (Figure 20) glass coverslips, as well as on a native PBM (Figure 21).

WT, *RhoA*^{-/-} and *Cdc42*^{-/-} MKs were all able to build up podosomes upon adhesion to these ECM proteins and the PBM, which was evident by dot-like F-actin-rich structures (Figure 19 A, 20 A, 21 A). Quantification of cell surface (µm²), total number of podosomes (n), size of podosomes (µm²) and podosomes per area (per µm²) (using ImageJ and a podosome counting macro[49]) revealed no significant alteration in podosome formation of *RhoA*^{-/-} and *Cdc42*^{-/-} MKs compared to their WT counterparts on fibrillar collagen I (Figure 19 B-F) or fibrinogen (Figure 20 B-F). Interestingly, *Cdc42*^{-/-} MKs exhibited decreased podosome size on PBM (0.30 ± 0.03 µm²) compared to WT MKs (0.48 ± 0.16 µm²) (Figure 21 B, E). All other parameters on this ECM surface were not significantly altered (Figure 21 B, C, D, F).

The high standard deviations in this experiment probably originated from the high variability of MK- and podosome sizes due to different stages of maturation and different levels of ploidy[55].
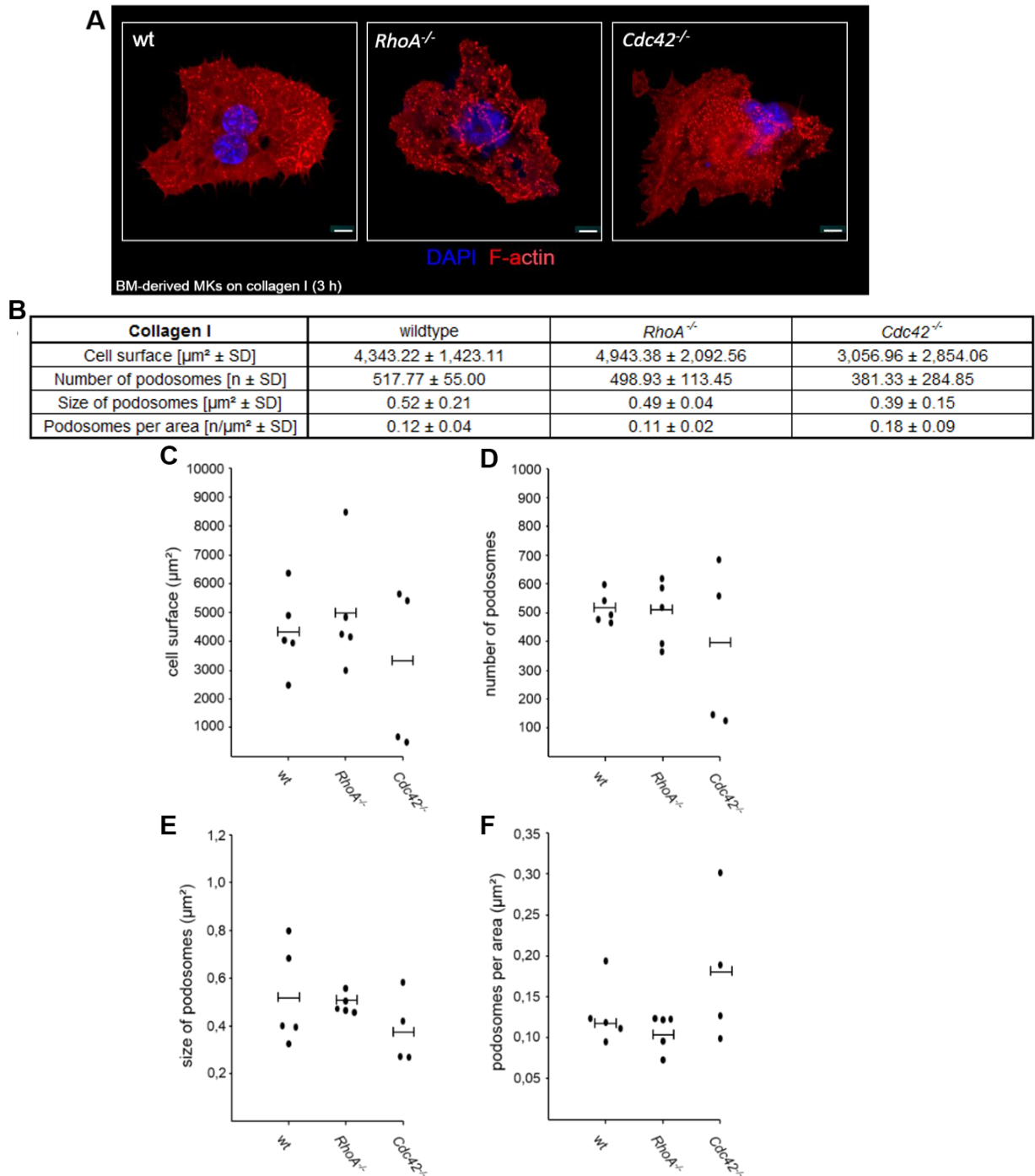
Collagen I	wildtype	RhoA⁻/⁻	Cdc42⁻/⁻
Cell surface [µm² ± SD]	4,343.22 ± 1,423.11	4,943.38 ± 2,092.56	3,056.96 ± 2,854.06
Number of podosomes [n ± SD]	517.77 ± 55.00	498.93 ± 113.45	381.33 ± 284.85
Size of podosomes [µm² ± SD]	0.52 ± 0.21	0.49 ± 0.04	0.39 ± 0.15
Podosomes per area [n/µm² ± SD]	0.12 ± 0.04	0.11 ± 0.02	0.18 ± 0.09

Figure 19: *RhoA⁻/⁻*- and *Cdc42⁻/⁻* MKs spread and form podosomes on collagen I.
BM-derived MKs were allowed to spread on fibrillar collagen I-coated (50 µg/ml) glass coverslips, incubated for 3 h and then fixed and stained with DAPI (blue) and for F-actin (red). (A) Representative immunofluorescence images were acquired with a Leica TCS SP5 confocal microscope (Leica Microsystems) using a 63x objective. Scale bars represent 10 µm. (B) Overview of measurements (cell surface in µm², number of podosomes, size of podosomes in µm² and podosomes per area (per µm²)) of all genotypes on collagen I. (C-F) Quantification of cell surface, number of podosomes, podosomes per area and size of podosomes of selected (spread) MKs. Data is presented in dot-plots plus mean of ≥ 3 analyzed MKs of ≥ 4 individuals. *P<0.05, **P<0.01, ***P<0.001 (Student's t-test)

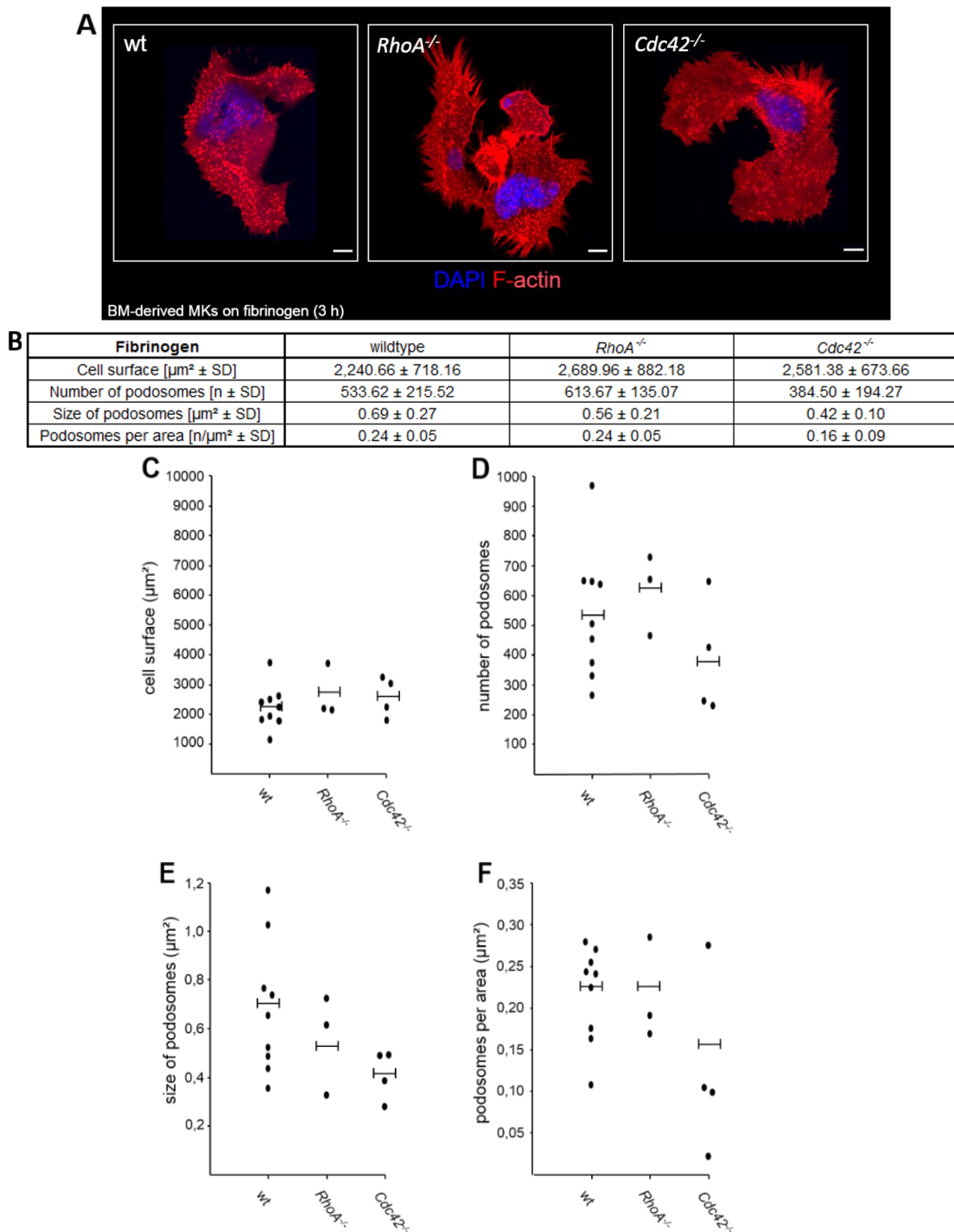| Fibrinogen	wildtype	RhoA⁻ᐟ⁻	Cdc42⁻ᐟ⁻
Cell surface [µm² ± SD]	2,240.66 ± 718.16	2,689.96 ± 882.18	2,581.38 ± 673.66
Number of podosomes [n ± SD]	533.62 ± 215.52	613.67 ± 135.07	384.50 ± 194.27
Size of podosomes [µm² ± SD]	0.69 ± 0.27	0.56 ± 0.21	0.42 ± 0.10
Podosomes per area [n/µm² ± SD]	0.24 ± 0.05	0.24 ± 0.05	0.16 ± 0.09

Figure 20: *RhoA⁻ᐟ⁻*- and *Cdc42⁻ᐟ⁻* **MKs spread and form podosomes on fibrinogen.**
BM-derived MKs were allowed to spread on fibrinogen-coated (100 µg/ml) glass coverslips, incubated for 3 h and then fixed and stained with DAPI (blue) and for F-actin (red). (A) Representative immunofluorescence images were acquired with a Leica TCS SP5 confocal microscope (Leica Microsystems) using a 63x objective. Scale bars represent 10 µm. (B) Overview of measurements (cell surface in µm², number of podosomes, size of podosomes in µm² and podosomes per area (per µm²)) of all genotypes on fibrinogen. (C-F) Quantification of cell surface, number of podosomes, podosomes per area and size of podosomes of selected (spread) MKs. Data is presented in dot-plots plus mean of ≥ 3 analyzed MKs of ≥ 3 individuals. *P<0.05, **P<0.01, ***P<0.001 (Student's t-test).

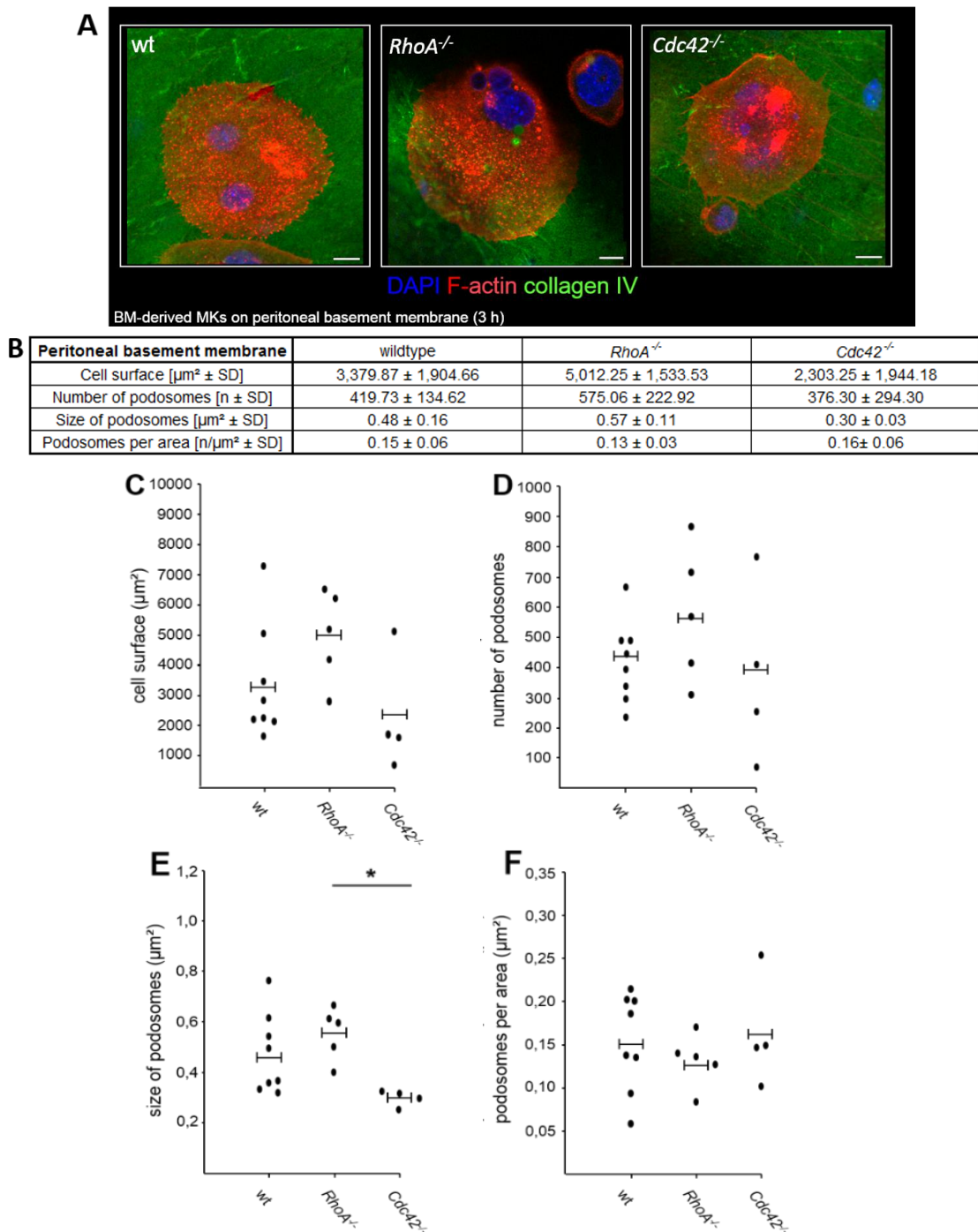**Figure 21: Moderate differences between WT, *RhoA⁻ᐟ⁻* and *Cdc42⁻ᐟ⁻* MKs regarding spreading and podosome formation on PBM.**
BM-derived MKs were allowed to spread on PBM, incubated for 3 h and then fixed and stained with DAPI (blue) and for F-actin (red) and collagen IV (green). (A) Representative immunofluorescence images were acquired with a Leica TCS SP5 confocal microscope (Leica Microsystems) using a 63x objective. Scale bars represent 10 µm. (B) Overview of measurements (cell surface in µm², number of podosomes, size of podosomes in µm² and podosomes per area (per µm²)) of all genotypes on PBM. (C-F) Quantification of cell surface, number of podosomes, podosomes per area and size of podosomes of selected (spread) MKs. Data is presented in dot-plots plus mean of ≥ 3 analyzed MKs of ≥ 4 individuals. *P<0.05, **P<0.01, ***P<0.001 (Student's t-test).

WT MKs displayed significant differences in cell surface area on the different used substrates. MKs on collagen I (4,343.22 ± 1,423.11 µm²) had larger surfaces compared to MKs on fibrinogen (2,240.66 ± 718.16 µm²). MK cell surface area on PBM (3,379.87 ± 1,904.66 µm²) was not significantly different compared to fibrinogen (Figure 22 A, B). Analysis of the cell surface area of *RhoA*^{-/-} MKs revealed difference. *RhoA*^{-/-} MKs were significantly larger upon adhesion on PBM (5,012.25 ± 1,533.53 µm²) than on fibrinogen (2,689.89 ± 882.81 µm²). MK cell surface area on collagen I (4,943.38 ± 2,092.56 µm²), however, was not significantly different compared to fibrinogen, which was probably due to the high variability in the assay (Figure 23 A, B). *Cdc42*^{-/-} MK surface area was similar on collagen I (3,056.96 ± 2,854.06 µm²), fibrinogen (2,581.38 ± 673.66 µm²) and PBM (2,303.25 ± 1,944.18 µm²) (Figure 24 A, B).

All analyzed genotypes showed both a comparable number and size of podosomes (Figures 22 A, C, D; 23 A, C, D; 24 A, C, D).

Podosome density (podosomes per area) of WT MKs on fibrinogen (0.24 ± 0.05 per µm²) was significantly increased compared to WT MKs on collagen I (0.12 ± 0.04 per µm²) and PBM (0.15 ± 0.06 per µm²) (Figure 22 A, E). Also *RhoA*^{-/-} MKs on collagen I (0.11 ± 0.02 per µm²) and on PBM (0.13 ± 0.03 per µm²) showed a lower podosome density compared to *RhoA*^{-/-} MKs on fibrinogen (0.24 ± 0.05 per µm²) (Figure 23 A, E). *Cdc42*^{-/-} MKs on collagen I (0.18 ± 0.09 per µm²), fibrinogen (0.16 ± 0.09 per µm²) and PBM (0.16 ± 0.06 per µm²) did not show any ECM-dependent alteration in podosome density (Figure 24 A, E).

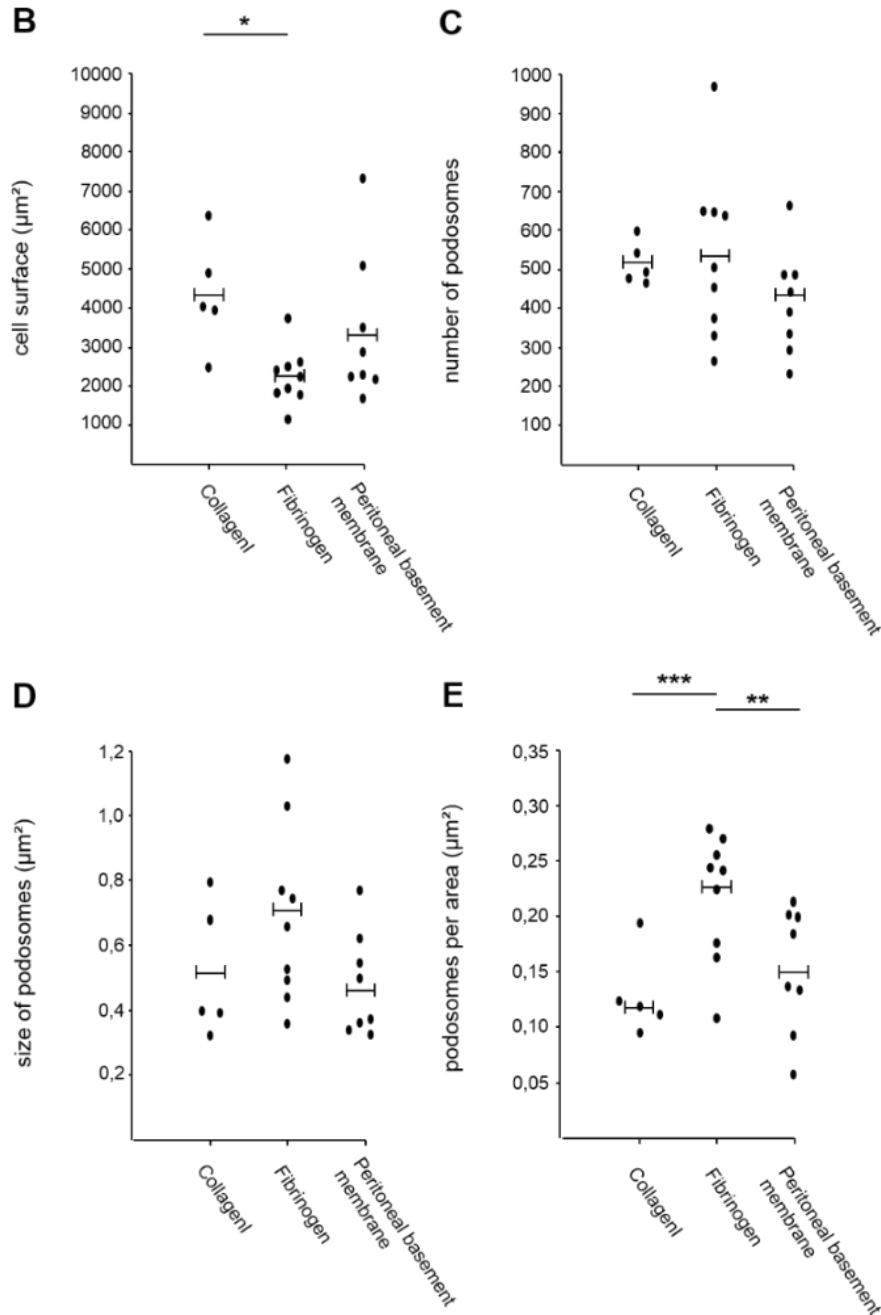| wildtype	Collagen I	Fibrinogen	Peritoneal basement membrane
Cell surface [µm² ± SD]	4,343.22 ± 1,423.11	2,240.66 ± 718.16	3,379.87 ± 1,904.66
Number of podosomes [n ± SD]	517.77 ± 55.00	533.62 ± 215.52	419.73 ± 134.62
Size of podosomes [µm² ± SD]	0.52 ± 0.21	0.69 ± 0.27	0.48 ± 0.16
Podosomes per area [n/µm² ± SD]	0.12 ± 0.04	0.24 ± 0.05	0.15 ± 0.06

Figure 22: WT MKs show increased cell surface area on collagen compared to fibrinogen and increased podosome density on fibrinogen compared to collagen I and PBM.
(A) shows a compilation of all investigated data (cell surface in µm², number of podosomes, size of podosomes in µm² and podosomes per area (per µm²)) of WT MKs. (B-E) show dot plots of this data on different ECM proteins (collagen I, fibrinogen, and PBM). Data is presented in dot-plots plus mean of ≥ 3 analyzed MKs of ≥ 3 individuals. *P<0.05, **P<0.01, ***P<0.001 (Student's t-test).

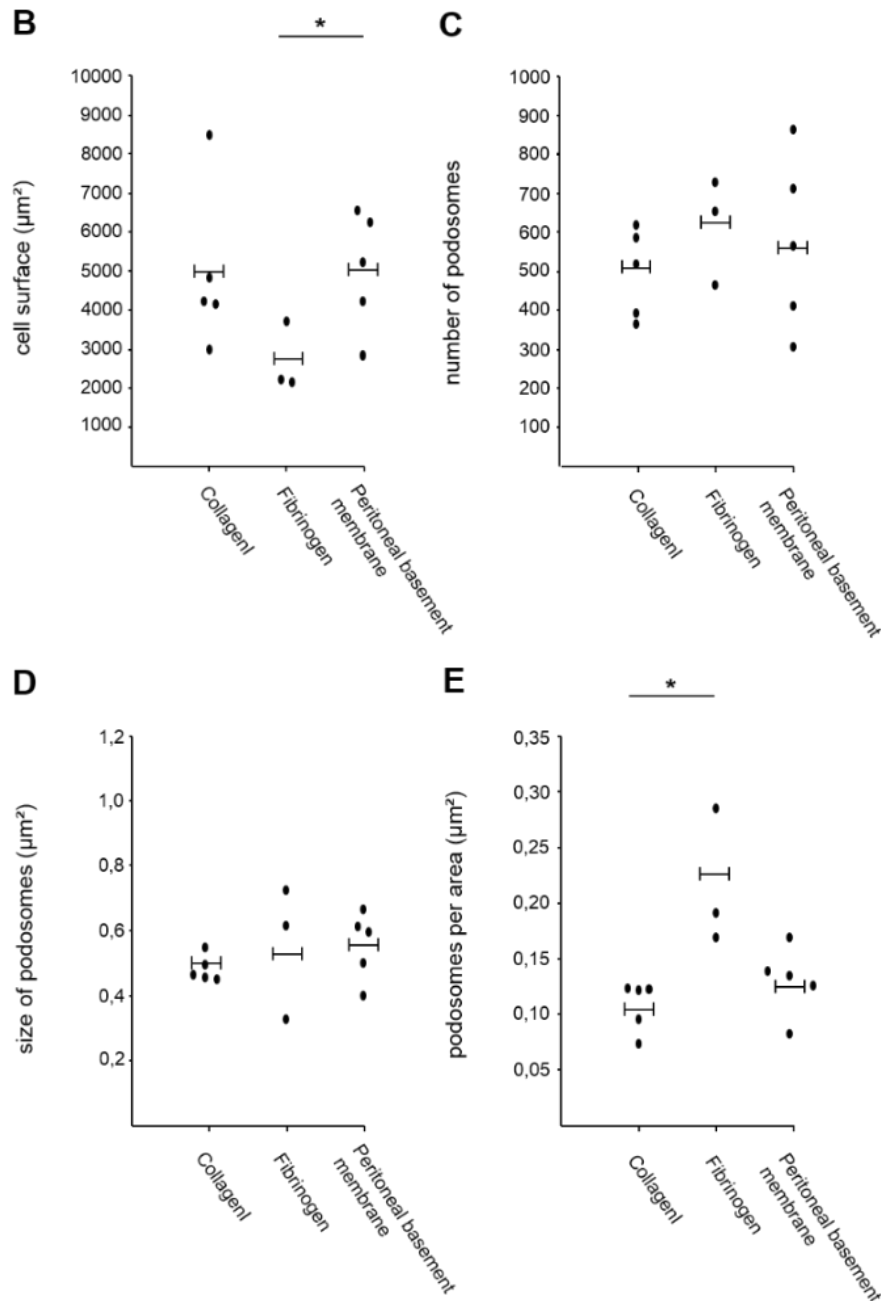| **RhoA** [-/-]	Collagen I	Fibrinogen	Peritoneal basement membrane
Cell surface [µm² ± SD]	4,943.38 ± 2,092.56	2,689.96 ± 882.18	5,012.25 ± 1,533.53
Number of podosomes [n ± SD]	498.93 ± 113.45	613.67 ± 135.07	575.06 ± 222.92
Size of podosomes [µm² ± SD]	0.49 ± 0.04	0.56 ± 0.21	0.57 ± 0.11
Podosomes per area [n/µm² ± SD]	0.11 ± 0.02	0.24 ± 0.05	0.13 ± 0.03

Figure 23: _RhoA_[-/-] MKs show increased cell surface area on PBM compared to fibrinogen, as well as increased density of podosomes on fibrinogen compared to collagen I.
(A) shows a compilation of all investigated data (cell surface in µm², number of podosomes, size of podosomes in µm² and podosomes per area (per µm²)) of _RhoA_[-/-] MKs. (B-E) show dot plots of this data on different ECM proteins (collagen I, fibrinogen, and PBM). Data is presented in dot-plots plus mean of ≥ 3 analyzed MKs of ≥ 3 individuals. *P<0.05, **P<0.01, ***P<0.001 (Student's t-test).

Cdc42⁻ᐟ⁻	Collagen I	Fibrinogen	Peritoneal basement membrane
Cell surface [µm² ± SD]	3,056.96 ± 2,854.06	2,581.38 ± 673.66	2,303.25 ± 1,944.18
Number of podosomes [n ± SD]	381.33 ± 284.85	384.50 ± 194.27	376.30 ± 294.30
Size of podosomes [µm² ± SD]	0.39 ± 0.15	0.42 ± 0.10	0.30 ± 0.03
Podosomes per area [n/µm² ± SD]	0.18 ± 0.09	0.16 ± 0.09	0.16± 0.06
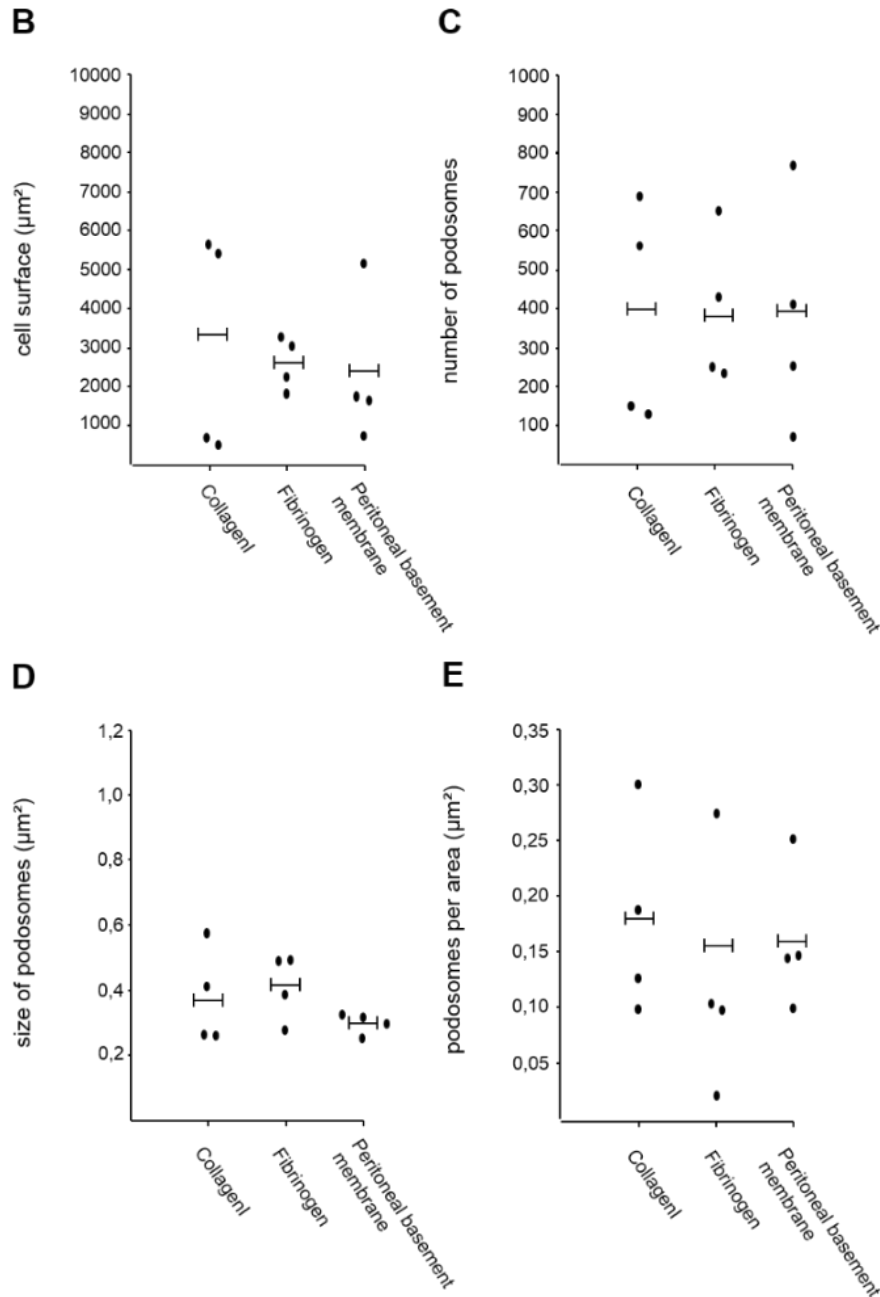
Figure 24: *Cdc42*⁻ᐟ⁻ MKs show comparable podosome formation on all tested substrates. (A) shows a compilation of all investigated data (cell surface in µm², number of podosomes, size of podosomes in µm² and podosomes per area (per µm²)) of *Cdc42*⁻ᐟ⁻ MKs. (B-E) show dot plots of this data on different ECM proteins (collagen I, fibrinogen, and PBM). Data is presented in dot-plots plus mean of ≥ 3 analyzed MKs of ≥ 3 individuals. *P<0.05, **P<0.01, ***P<0.001 (Student's t-test).

3.2.2 Involvement of tyrosine kinases in podosome formation

Upon contact with extracellular collagen, platelets adhere and become activated[56]. This process is thought to be triggered by the membrane-attached receptors integrin α2β1, including signal transducer Src, as well as GPVI which itself includes signal transducers Fyn, Lyn (Src-kinases) and Syk.

Tyrosine kinase Src is known to be an important player in signaling pathways downstream of GPVI, Integrin α2β1 and integrin αIIbβ3 in platelets. Spleen tyrosine kinase Syk is also described as an important signal transducer in the GPVI-pathway. Syk activation induces platelet aggregation, Ca^{2+}-mobilization, integrin activation and degranulation. Platelet activation induced by tyrosine kinases is accompanied by pronounced cytoskeletal reorganization, which might occur also in MKs.

To therefore investigate the involvement of Src-kinases in podosome formation, BM-derived WT MKs were allowed to spread on collagen I and fibrinogen in the presence or absence of the Src-kinase inhibitor PP2 or its inactive control PP3.

On collagen I, vehicle treated WT MKs were able to form individual podosomes and typical podosome belt superstructures along collagen I fibres (Figure 25 A). Treatment of MKs with PP3 revealed no alteration in spreading or podosome formation (Figure 25 B). By marked contrast, podosome formation was virtually abolished upon treatment of WT MKs with PP2 (Figure 25 C).

Figure 25: Src-kinase inhibitor PP2 abolishes spreading and podosome formation of WT MKs on collagen I.
BM-derived MKs were allowed to spread on fibrillar collagen I-coated (50 µg/ml) glass coverslips, incubated for 3 h and then fixed and stained with DAPI (blue) and for F-actin (red). Shown images are representative of untreated (A), PP3- (B) and PP2-treated (C) WT MKs. Immunofluorescence images were acquired with a Leica TCS SP5 confocal microscope (Leica Microsystems) using a 63x objective. Scale bars represent 10 µm. Amount of data: ≥ 3 analyzed MKs of 5 individuals.

Similar results were observed for MKs spread on fibrinogen. Here, vehicle- or PP3-treated WT MKs partially spread and/or formed individual podosomes (Figure 26 A,B). In contrast, PP2 treatment strongly inhibited spreading and podosome formation (Figure 26 C).
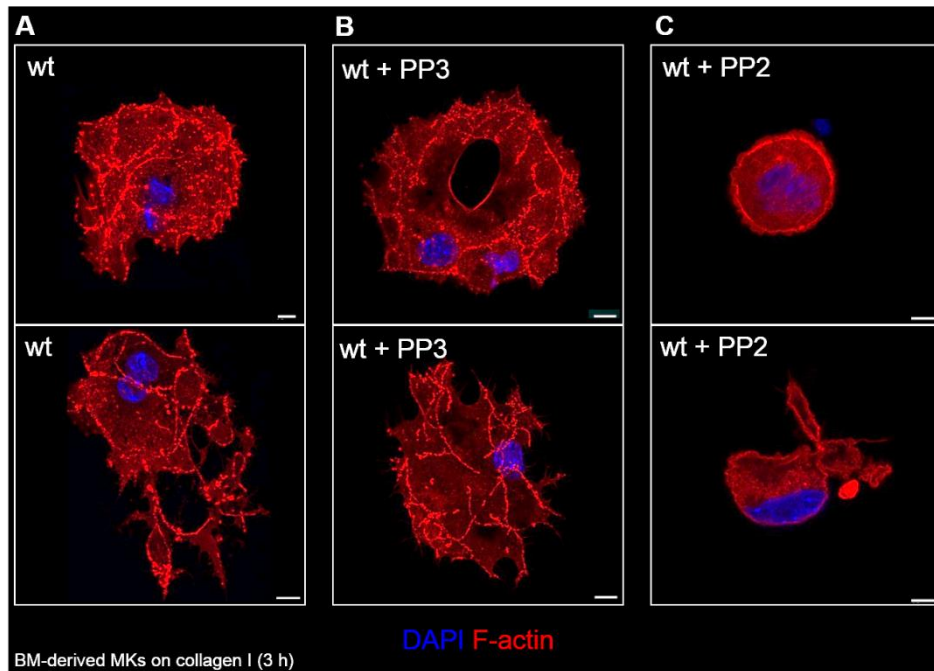

Figure 26: Src-kinase inhibitor PP2 strongly reduces spreading and podosome formation of WT MKs on fibrinogen.
BM-derived MKs were allowed to spread on fibrinogen-coated (100 µg/ml) glass coverslips, incubated for 3 h and then fixed and stained with DAPI (blue) and for F-actin (red) and α-tubulin (green). Shown images are representative of untreated (A), PP3- (B) and PP2-treated (C) WT MKs. Immunofluorescence images were acquired with a Leica TCS SP5 confocal microscope (Leica Microsystems) using a 63x objective. Scale bars represent 10 µm. Amount of data: ≥ 2 analyzed MKs of 3 individuals.

In order to investigate in the influence intensivity of the enzyme spleen tyrosine kinase Syk on podosome formation in MKs, WT MKs were treated with the selective Syk inhibitor R406 and spreading on collagen I, as well as fibrinogen was compared to untreated MKs.

In line with the results shown above, vehicle treated WT MKs were able to form individual podosomes, as well as podosome belt superstructures along the collagen fibers (Figure 27 A), whereas these processes were markedly reduced upon treatment with R406 (Figure 27 B).

Figure 27: Syk-tyrosine-kinase inhibitor R406 strongly reduces spreading and podosome formation of WT MKs on collagen I.
BM-derived MKs were allowed to spread on fibrillar collagen I-coated (50 µg/ml) glass coverslips, incubated for 3 h and then fixed and stained with DAPI (blue) and for F-actin (red). Shown images are representative of untreated (A), R406-treated (B) WT MKs. Immunofluorescence images were acquired with a Leica TCS SP5 confocal microscope (Leica Microsystems) using a 63x objective. Scale bars represent 10 µm. Amount of data: ≥ 3 analyzed MKs of 5 individuals.

On fibrinogen, vehicle-treated WT MKs formed individual podosomes (Figure 28 A). In contrast, R406 treated cells were strongly inhibited in spreading and podosome formation (Figure 28 B).

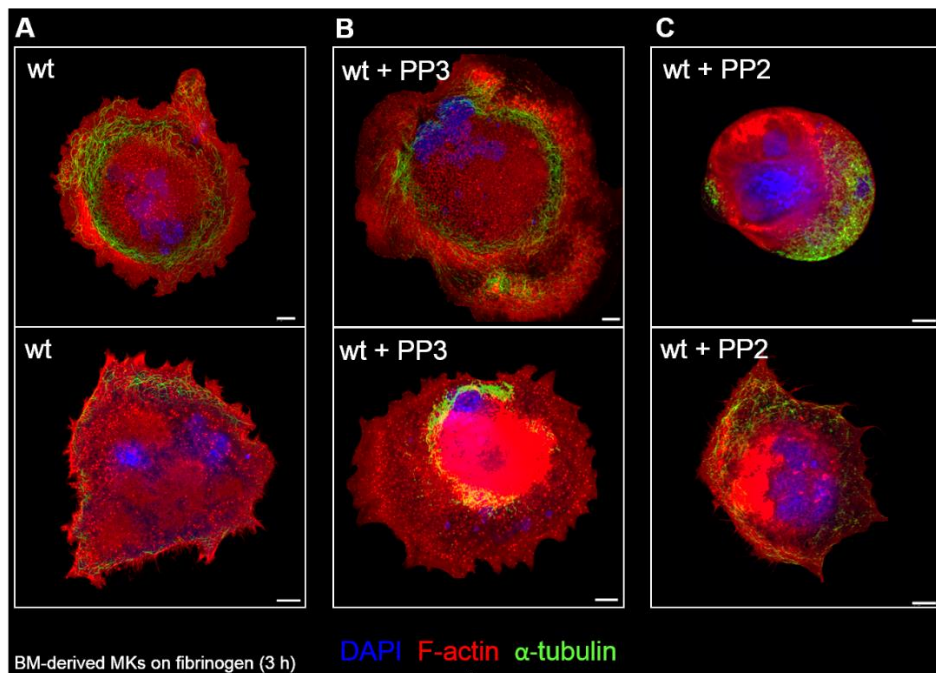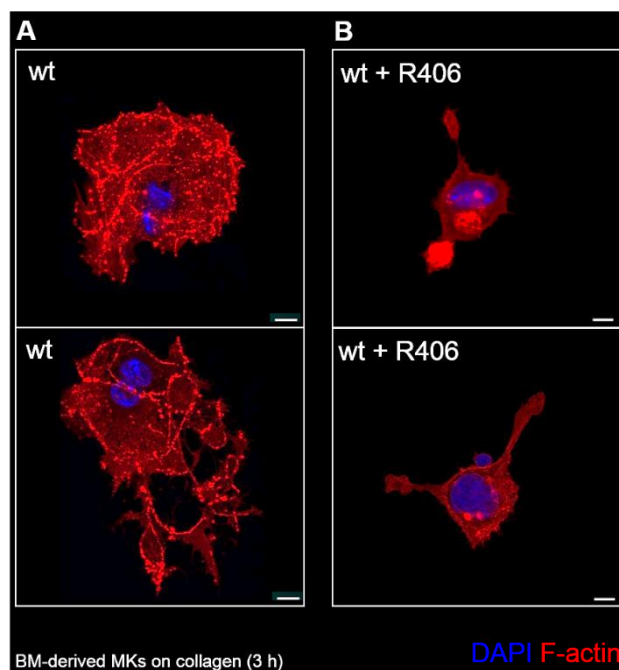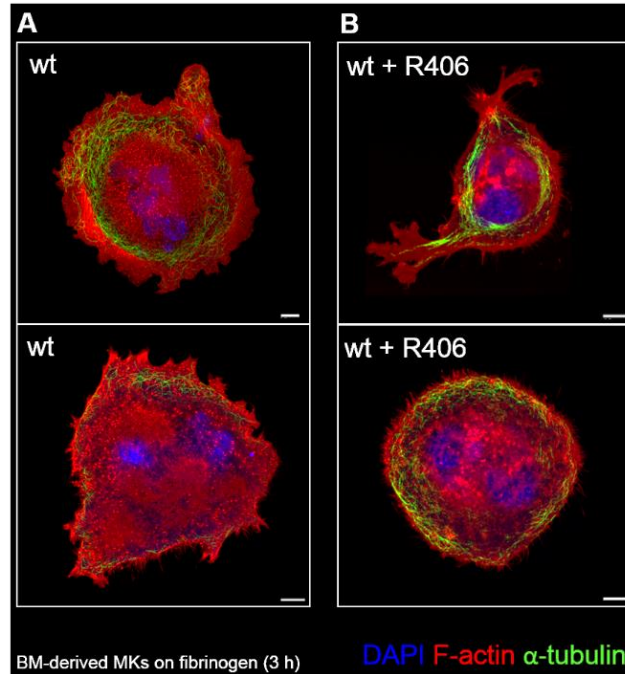**Figure 28: Syk-tyrosine-kinase inhibitor R406 strongly reduces spreading and podosome formation of WT MKs on fibrinogen.**
BM-derived MKs were allowed to spread on fibrinogen-coated (100 µg/ml) glass coverslips, incubated for 3 h and then fixed and stained with DAPI (blue) and for F-actin (red). Shown images are representative of untreated (A) and R406-treated (B) WT MKs. Immunofluorescence images were acquired with a Leica TCS SP5 confocal microscope (Leica Microsystems) using a 63x objective. Scale bars represent 10 µm. Amount of data: ≥ 2 analyzed MKs of 3 individuals.

While it is important to note that side effects of inhibitor treatment have not yet been ruled out, the performed experiments indicate that Src and Syk play significant roles in MK podosome formation.

In the next step podosome formation of BM-derived MKs from $Syk^{-/-}$ mice upon adhesion on collagen I and fibrinogen was analyzed.

Strikingly, knock-out of Syk phenocopied R406 treatment and virtually abolished spreading and podosome formation in MKs obtained by lineage depletion (see 2.2.1.1) (Figure 29 A, B top).

Interestingly however, *Syk*$^{-/-}$ MKs obtained by the enrichment method (see 2.2.1.2) exhibited a different phenotype in this assay. In general, the surface area of WT MKs was increased and single podosome formation as well as podosome belts were more pronounced (Figure 29 A bottom). Surprisingly, *Syk*$^{-/-}$ MKs exhibited a morphology similar to the WT, being able to spread and form podosomes (Figure 29 B bottom). Thus, the choice of the MK culture method dramatically affected spreading and podosome formation in WT and particularly *Syk*$^{-/-}$ MKs.
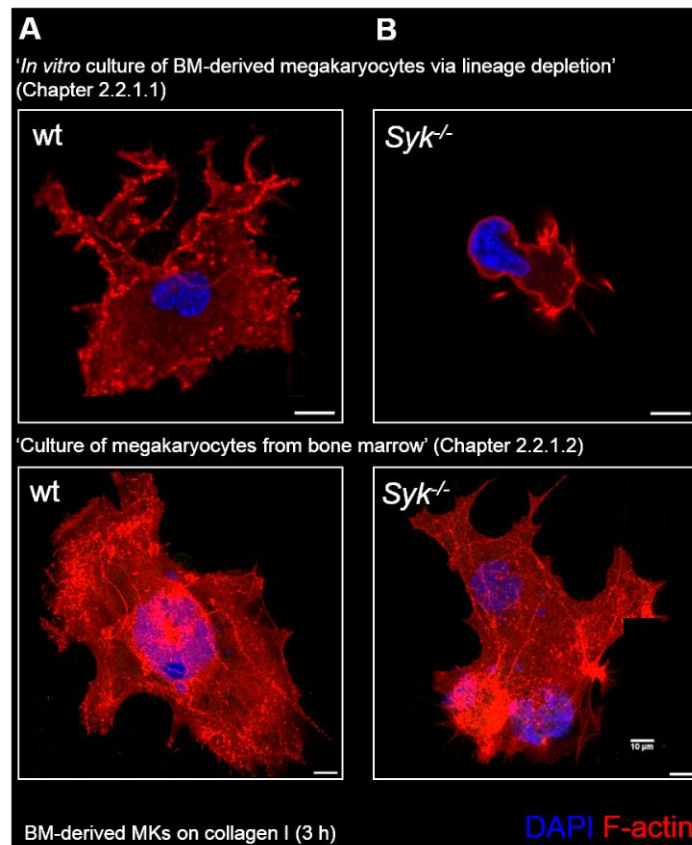
Figure 29: Depending on the culture method, *Syk*$^{-/-}$ MKs display normal, or strongly reduced spreading and podosome formation on collagen I.
BM-derived MKs were allowed to spread on fibrillar collagen I-coated (50 µg/ml) glass coverslips, incubated for 3 h and then fixed and stained with DAPI (blue) and for F-actin (red). Shown images are representative of WT (A) and *Syk*$^{-/-}$ (B) WT MKs. Immunofluorescence images were acquired with a Leica TCS SP5 confocal microscope (Leica Microsystems) using a 63x objective. Scale bars represent 10 µm. Amount of data: (A top, B top) ≥ 3 analyzed MKs of 3 individuals; (A bottom, B bottom) ≥ 4 analyzed MKs of 2 individuals.

Fibrinogen binding to activated Integrin αIIbβ3 in platelets induces signaling that involves both Src and Syk. However, podosome formation of $Syk^{-/-}$ MKs on fibrinogen was not reduced compared to WT MKs obtained by either of the two culture methods. In both experiments, proper spreading and podosome formation was observed, indicating that Syk plays no role in these processes in signaling induced by fibrinogen. Interestingly, MK morphology was generally different between the two culture systems. MKs obtained by lineage depletion (Chapter 2.2.1.1) (Figure 30 A top, B top) were overall smaller and exhibited more filopodia-like structures compared to those obtained with the enrichment method (Chapter 2.2.1.2) (Figure 30 A bottom, B bottom) which displayed bigger cells with round cell borders. Additionally, podosome formation in MKs obtained by lineage depletion seemed to be overall increased.

Figure 30: Syk-deficiency does not affect MK spreading and podosome formation on fibrinogen.
BM-derived MKs were allowed to spread on fibrinogen-coated (100 µg/ml) glass coverslips, incubated for 3 hours and then fixed and stained with DAPI (blue) and for F-actin (red). Shown images are representative of WT (A) and $Syk^{-/-}$ (B) WT MKs. Immunofluorescence images were acquired with a Leica TCS SP5 confocal microscope (Leica Microsystems) using a 63x objective. Scale bars represent 10 µm. Amount of data: ≥ 3 analyzed MKs of 3 individuals.

3.3.3 Involvement of GPVI in podosome formation

Binding of platelet GPVI to collagen exposed upon vessel injury represents a crucial event for the initiation of platelet activation in hemostasis and thrombosis. Different collagen types are present in the BM leading to the possibility that GPVI signaling also plays a role in MKs.

To investigate the importance of GPVI in podosome formation, MKs from mice obtained by lineage depletion were allowed to spread on collagen I. In addition, spreading of $Gp6^{-/-}$ MKs on fibrinogen was also investigated. Notably, spreading area and podosome formation of $Gp6^{-/-}$ MKs were unaltered on collagen I and fibrinogen compared to the WT (Figure 31, 32). These findings approve the existence of alternative signaling pathways on both collagen I and fibrinogen. It has to be noted, however, in this assay only successfully spread MKs were analyzed.

Figure 31: GPVI-deficiency does not affect MK spreading area and podosome formation on collagen I.
BM-derived MKs were allowed to spread on fibrillar collagen I-coated (50 µg/ml) glass coverslips, incubated for 3 h and then fixed and stained with DAPI (blue) and for F-actin (red). Shown images are representative of WT (A) and $Gp6^{-/-}$ (B) WT MKs. Immunofluorescence images were acquired with a Leica TCS SP5 confocal microscope (Leica Microsystems) using a 63x objective. Scale bars represent 10 µm. Amount of data: 3 analyzed MKs of 3 individuals.
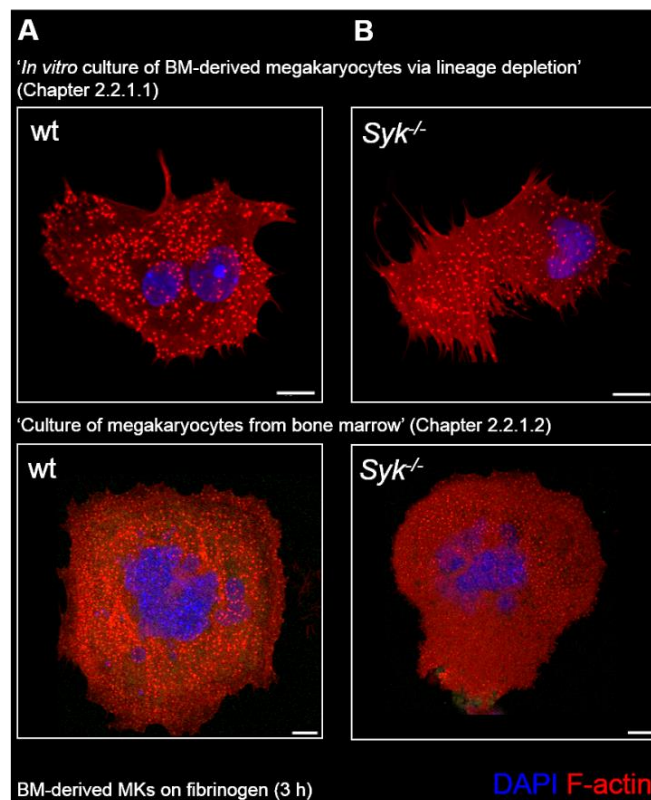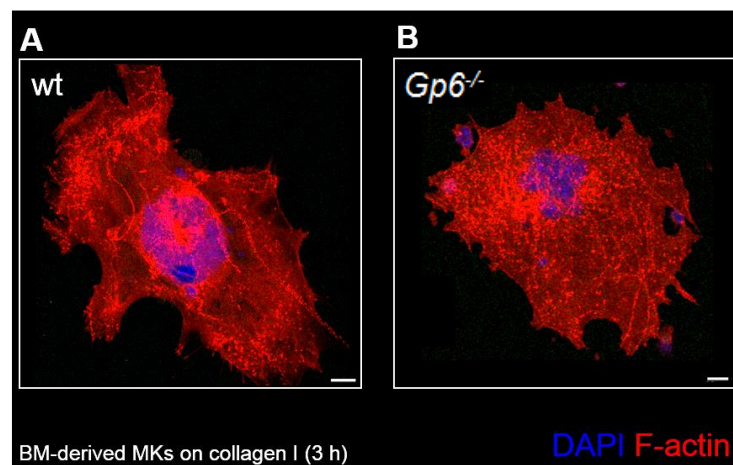
Figure 32: GPVI-deficiency does not affect MK spreading and podosome formation on fibrinogen.
BM-derived MKs were allowed to spread on fibrinogen-coated (100 µg/ml) glass coverslips, incubated for 3 h and then fixed and stained with DAPI (blue) and for F-actin (red). Shown images are representative of WT (A) and $Gp6^{-/-}$ (B) WT MKs. Immunofluorescence images were acquired with a Leica TCS SP5 confocal microscope (Leica Microsystems) using a 63x objective. Scale bars represent 10 µm. Amount of data: 3 analyzed MKs of 3 individuals.
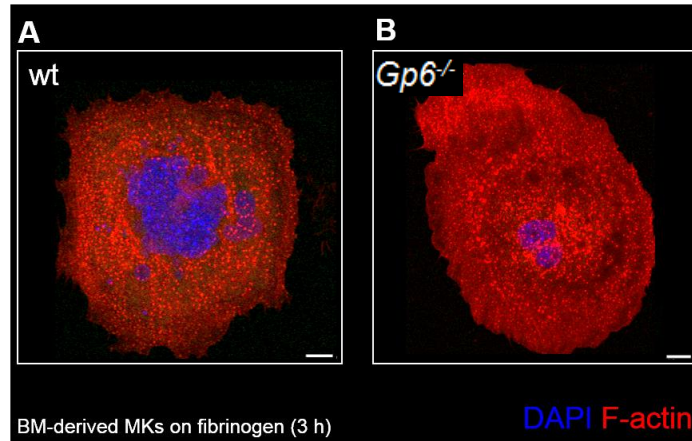
3.3.4 Quantitative analysis of the involvement of Syk and GPVI on MK spreading

As shown above, $Gp6^{-/-}$ and $Syk^{-/-}$ MKs were still able to spread and polarize. Interestingly, depending on the genotype, some coverslips seemed covered with many spread MKs while on other coverslips such MKs were harder to find.

Therefore, immunofluorescence images at low magnification (10x) of WT MKs and MKs derived from $Syk^{-/-}$ or $Gp6^{-/-}$ mice seeded on collagen I and fibrinogen were taken and analyzed by comparing the proportion of spread MKs (n > 50 cells). On collagen 72.34 ± 5.34 % of WT MKs spread (Figure 33 A,D), whereas only 36.78 ± 4.25 % (p < 0.001) of $Syk^{-/-}$ MKs (Figure 33 B,D) and 20.59 ± 2.58 % (p < 0.001) of $GP6^{-/-}$ MKs (Figure 33 C,D) displayed spreading, revealing major defects in these cells.

On fibrinogen, 27.39 ± 1.38 % of WT MKs spread (Figure 34 A,D), while only 14.01 ± 1.74 % (p < 0.001) of $Syk^{-/-}$ MKs (Figure 34 B,D) showed comparable spreading. However, 25.79 ± 1.23 % (p = 0.15) of $GP6^{-/-}$ MKs spread on fibrinogen, excluding a role of GPVI in this assay.

MKs on collagen I generally displayed extremely rough, jagged cell borders, whilst fibrinogen triggered a more roundish appearance of the cells.
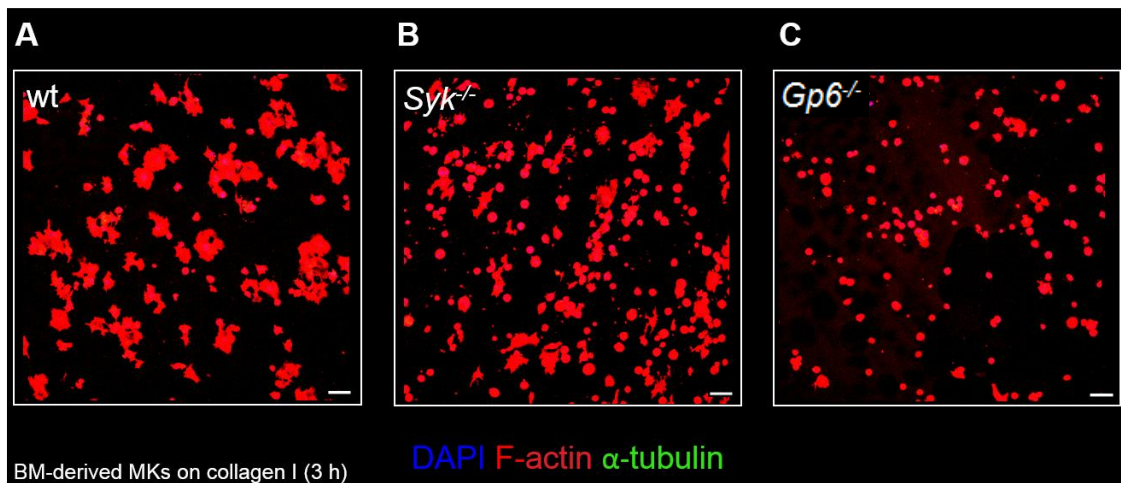
Figure 33: Relative number of spread *Syk*^{-/-} and *Gp6*^{-/-} MKs on collagen I is reduced.
(A-C) BM-derived MKs were allowed to spread on collagen I-coated (50 µg/ml) glass coverslips, incubated for 3 h and then fixed and stained with DAPI (blue) and for F-actin (red) and α-tubulin (green). Representative immunofluorescence images were acquired with a Leica TCS SP5 confocal microscope (Leica Microsystems) using a 10x objective. Overexposure was adjusted in ImageJ to ensure complete inspection of all F-actin structures. Scale bars represent 100 µm. (D) Bar graph quantification of relative amount of spread MKs on collagen I. Results are mean percentile of spread MKs ± SD of > 50 analyzed MKs of ≥ 3 individuals. *P<0.05, **P<0.01, ***P<0.001 (Student's t-test).
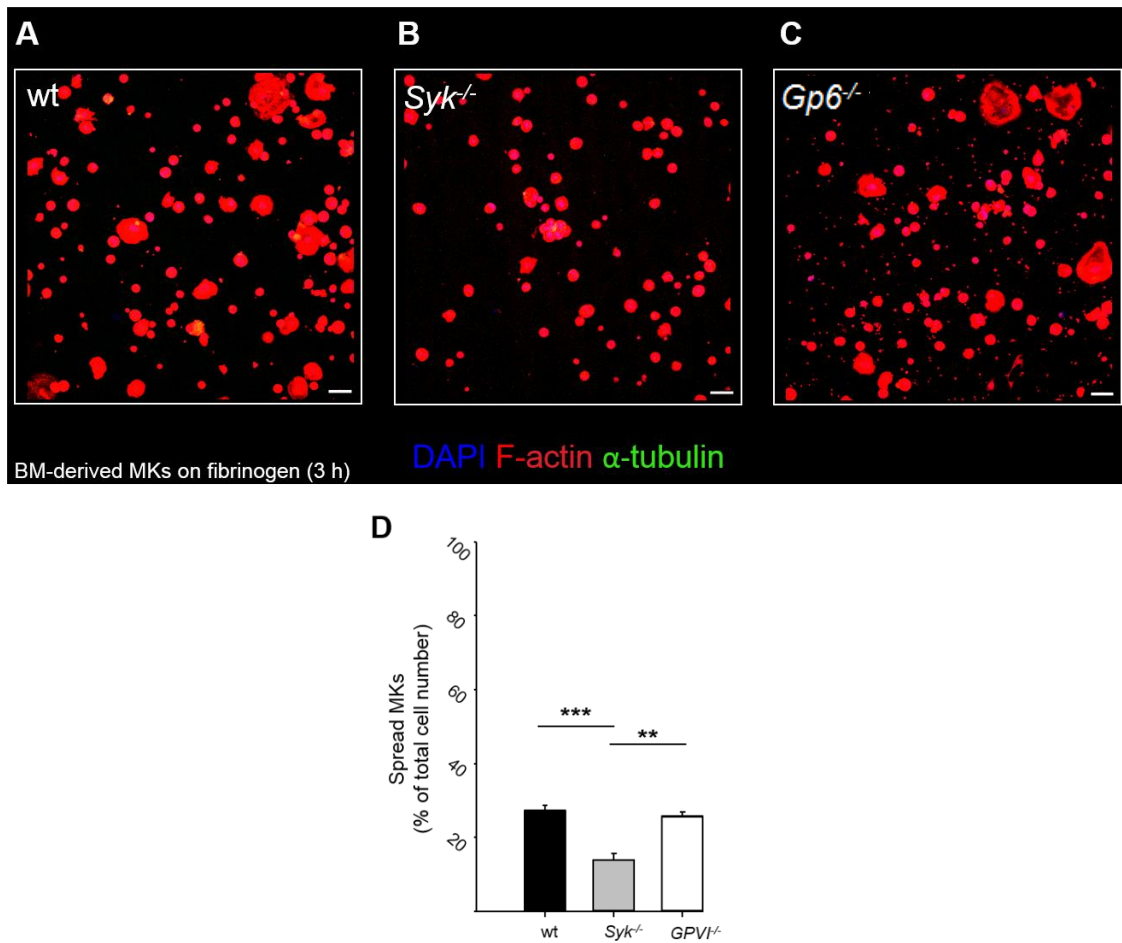
Figure 34: *Syk⁻ᐟ⁻*, but not *Gp6⁻ᐟ⁻* MKs show reduced spreading on fibrinogen.
(A-C) BM-derived MKs were allowed to spread on fibrinogen-coated (100 μg/ml) glass coverslips, incubated for 3 h and then fixed and stained with DAPI (blue) and for F-actin (red) and α-tubulin (green). Representative immunofluorescence images were acquired with a Leica TCS SP5 confocal microscope (Leica Microsystems) using a 10x objective. Overexposure was adjusted in ImageJ to ensure complete inspection of all F-actin structures. Scale bars represent 100 μm. (D) Bar graph quantification of relative amount of spread MKs on fibrinogen. Results are mean percentile of spread MKs ± SD of > 50 analyzed MKs of ≥ 3 individuals. *P<0.05, **P<0.01, ***P<0.001 (Student's t-test).

3.3.5 Involvement of MMPs in ECM-degradation by MKs

It has been described for different cell types that invadosome driven degradation of ECM components is mediated by secretion of MMPs. This process is thought to be required for cells to dissolve macromolecules in order to migrate into a desired direction and, as it is the case for MKs, to gain access to the inside of the vascular system for the purpose of platelet release[33].

For this thesis, a previously described fibrinogen degradation assay[29] was established. MKs were seeded on glass coverslips precoated with 'Alexa Fluor® 488 conjugated fibrinogen' and incubated for 3 h. After F-actin and DAPI staining, fluorescence intensities of areas without MK contact (with intact and fully fluorescent fibrinogen) were compared to areas with direct cell contact. (Figure 35).

Figure 35: BM-derived MKs degrade fibrinogen.
BM-derived MKs were allowed to spread on 'Alexa Fluor® 488 Conjugat'-coated glass coverslips, incubated for 3 h and then fixed and stained with DAPI (blue) and for F-actin (red). 3D stacks were acquired by immunofluorescent confocal microscopy. (A-C) show one XY plane of a representative Z-stack with labeled F-actin (A), fibrinogen (B) and the overlay of these two images (C). (D) shows F-actin and fibrinogen distribution in Z direction along the line indicated in C. Representative immunofluorescence images (A-C) and Z-stack images (D; glass slide with coating on top, MK below) were acquired with a Leica TCS SP5 confocal microscope (Leica Microsystems) using a 63x objective. Scale bars represent 10 µm. Images are representative for results of ≥ 5 analyzed individuals.

Confluent dark spots (Figure 35 B) represent areas absent of 'Alexa Fluor® 488 conjugated fibrinogen'. They were found directly underneath MKs and in areas in close vincinity. Lateral analysis of cellular morphology by Z-stack aquisition, showed that F-actin-rich structures (Figure 35 D at the bottom) protruded into the green labeled fibrinogen coating (Figure 35 D at the top). Furthermore, intense dots of fluorescent fibrinogen near large areas of degraded fibrinogen (Figure 36 white arrows) indicated increased fibrinogen accumulation in these areas.
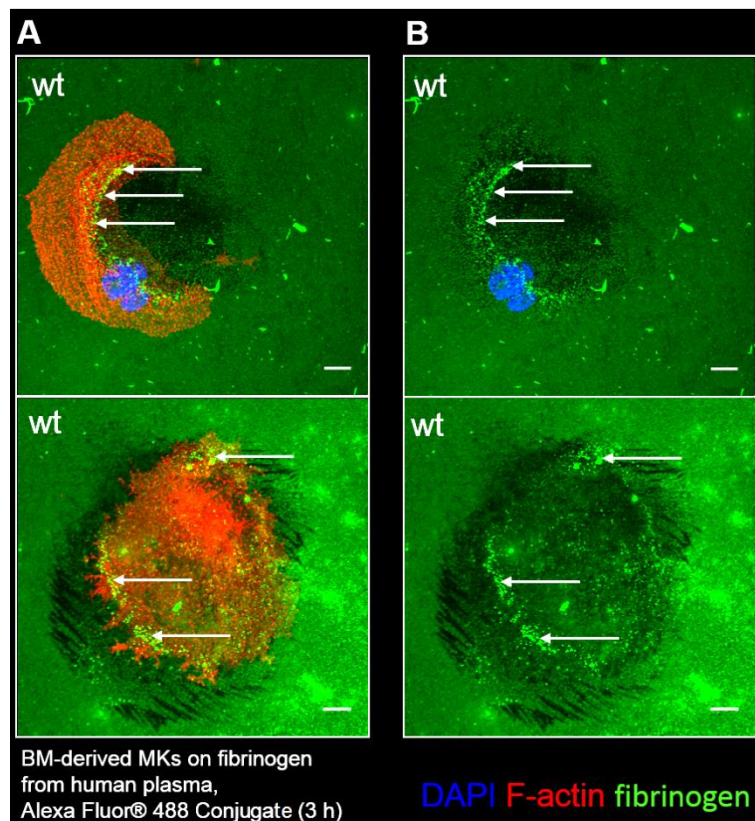
Figure 36: Fibrinogen accumulates near areas of intense fibrinogen degradation.
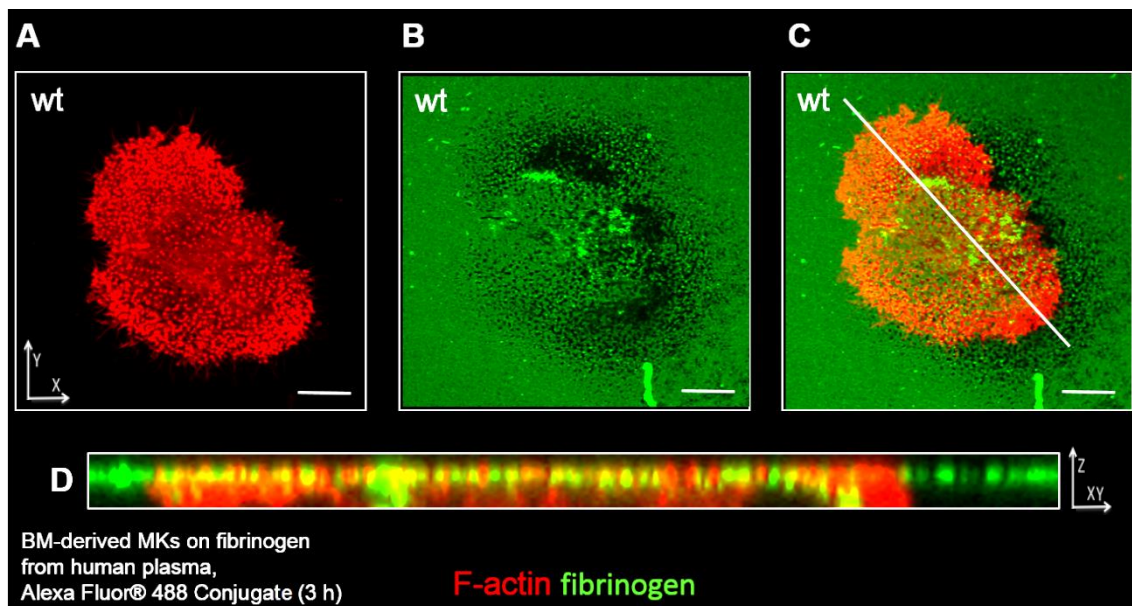BM-derived MKs were allowed to spread on an 'Alexa Fluor® 488 Conjugat'-coated glass coverslips, incubated for 3 h and then fixed and stained with DAPI (blue) and for F-actin (red). Immunofluorescence merge images including DAPI-, F-actin- and fibrinogen-staining (A) and solely including DAPI- and fibrinogen-staining (B) were acquired with a Leica TCS SP5 confocal microscope (Leica Microsystems) using a 63x objective. Scale bars represent 10 µm. Images are representative for results of ≥ 3 analyzed MKs of ≥ 5 individuals.

Figure 37 shows that decreased fluorescence in the fibrinogen coating was not caused by light interference underneath and close to F-actin structures. Areas of degraded fibrinogen were visible underneath labeled F-actin structures, as well as outside of these areas (Figure 37 A top, B top). Cells in an early stage of podosome formation, which did not yet degrade extracellular fibrinogen revealed intact fibrinogen (green) underneath F-actin structures (red, Figure 37 A bottom, B bottom).
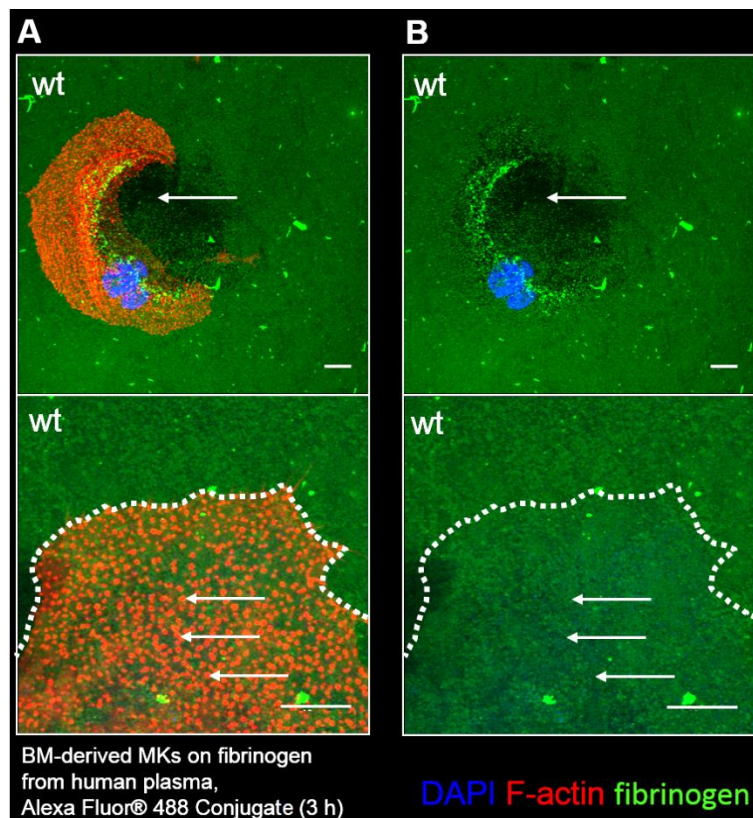
Figure 37: Dark spots are areas of degraded fibrinogen.
BM-derived MKs were allowed to spread on an 'Alexa Fluor® 488 Conjugat'-coated glass coverslips, incubated for 3 h and then fixed and stained with DAPI (blue) and for F-actin (red). Representative immunofluorescence merge images including DAPI-, F-actin and fibrinogen-staining (A) or only DAPI- and fibrinogen-staining (B) were acquired with a Leica TCS P5 confocal microscope (Leica Microsystems) using a 63x objective. Scale bars represent 10 µm. Images are representative for results of ≥ 5 analyzed individuals.

Inhibition of MMPs through GM6001, a broad spectrum matrixmetalloproteinase inhibitor, was measured by comparing fibrinogen degradation of GM6001-treated to untreated MKs (Figure 38). While the data variability was high, these preliminary experiments indicate that GM6001 treatment does not significantly affect fibrinogen degradation, which stands in contrast to previous findings [29]. Of note, similar results were obtained for *RhoA*-/- MKs.
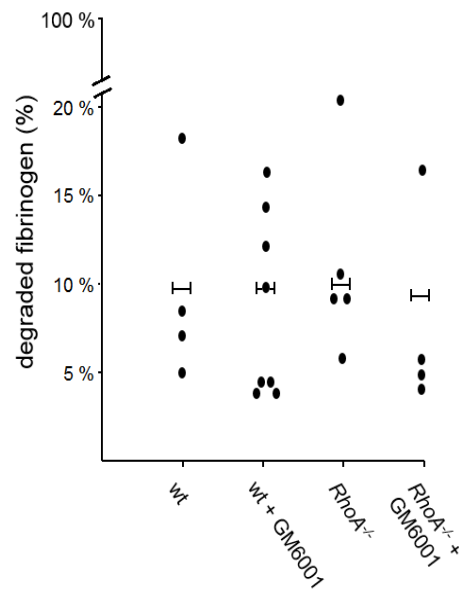
Figure 38: MMPs do not seem to be required for ECM degradation.
Neither WT, nor *RhoA*-/- MKs display alteration in fibrinogen degradation in the presence of GM6001. Data is presented in degraded area of fibrinogen (%) beneath MKs compared to undegraded area of fibrinogen. ≥ 3 analyzed MKs of ≥ 4 individuals. *P<0.05, **P<0.01, ***P<0.001 (Student's t-test).

4 DISCUSSION

Platelet activation and aggregation is essential to limit excessive blood loss at sites of vascular injury. On the other hand, uncontrolled thrombus formation has to be prevented since this may lead to complete vessel occlusion resulting in ischemic stroke or myocardial infarction, which are both leading causes of death worldwide[57-60]. Dysregulation of these processes can lead to severe bleeding disorders that can often be attributed to specific gene defects, resulting in impaired platelet function and/or platelet production (e.g. Glanzmann's thrombastenia[61] or Bernard-Soulier syndrome[62,63].) A more detailed understanding of platelet biogenesis and function is required for the search of new approaches in therapy.

Rho GTPases RhoA, Cdc42 and Rac1 are involved in cytoskeletal rearrangements, as well as in activatory and secretory processes in platelets and MKs[37,40,64]. In this thesis, findings on the involvement of RhoA and Cdc42 in polarization and podosome formation of terminally differentiated, mature MKs are presented.

4.1 MK Polarization

The exact mechanisms of transendothelial PPF by mature MKs in the BM *in vivo* are still poorly understood, but have recently been shown to involve cell polarisation[65].

In vitro analysis of polarization parameters in BM-derived MKs (WT, *RhoA^{-/-}* and *CDC42^{-/-}*) and Meg01 cells upon adhesion on fibronectin without additional (stimulative or inhibitive) supplement did not indicate polarization detectable by changes in the F-actin or tubulin cytoskeleton. In contrast, recent findings from our group employing a different assay not involving adhesive substrates revealed that Cdc42 induced and RhoA inhibited polarization of the MK DMS[65]. Previous studies show that staurosporin treated Meg 01 cells polarize on fibronectin[66]. This indicates the need of additional stimulative supplements to enable polarization in MKs and Meg 01 cells on fibronectin.

Interestingly, while untreated K562 cells showed minor signs of polarization upon adhesion on fibronectin, these features were much more pronounced in PMA induced WT and *RhoA*^{-/-} K562 cells. Western blot analysis confirmed RhoA deficiency in PMA-treated *RhoA*^{-/-} K562 cells, but strikingly revealed that RhoA was also strongly downregulated in WT K562 cells treated with PMA. These findings are in line with our results[65] and strongly suggest that the pronounced polarization in PMA-treated WT and *RhoA*^{-/-} cells is in both cases due to the absence of inhibitory signaling by the GTPase.

Previous studies indicate that BM stroma cells supply MKs with many proplatelet inhibiting signals. As soon as the MK touches a sinusoidal wall, inhibitory signals in this region are missing and the unipolar protrusions are built up[67,68]. In future studies, it will be crucial to investigate which upstream signaling regulates RhoA-mediated inhibition of polarization in MKs. Rac1 would be a potential candidate as its hyperactivity in *RhoA*^{-/-} cell lines was shown to be associated with increased presence lamellopodia protrusions[69]. However, our results reveal that concomitant knock-out of *Rac1* in *RhoA*^{-/-} MKs could not revert the phenotype evoked by RhoA deficiency, arguing against this signaling pathway in MKs.

In the context of this thesis, further studies *on Cdc42*^{-/-} and *Rac1*^{-/-} K562 cells, as well as immunofluorescent staining of additional proteins, like e.g. the microtubule organizing center (MTOC) or the golgi-complex in the here presented assays could reveal interesting findings.

4.2 Podosome formation

Formation of podosomes was proposed to be important in MKs to complete maturation and to release platelets into the blood stream[29]. Loss of the cytoskeletal regulators RhoA and Cdc42[37,40,70,71], may lead to alteration of intracellular F-actin and tubulin polymerization and thus may affect podosome formation.

In this thesis, podosome formation of WT, *RhoA*^{-/-}, *Cdc42*^{-/-} MKs on different ECM proteins (collagen I, fibrinogen and PBM) were analyzed by assessing different parameters, such as cell surface area, size, number and density of podosomes.

MKs of all genotypes formed podosomes on the used substrates. However, podosome size in $Cdc42^{-/-}$ MKs incubated on PBM was significantly reduced. Thus, while these results acknowledge $Cdc42^{-/-}$ as a potential player in podosome formation of MKs, the hypothesis that the GTPase is indispensable for podosome formation[32] is not supported.

The importance of Src-kinases and tyrosine kinase Syk in podosome formation of MKs was tested by pharmacological inhibition with PP2 and R406 on ECM substrates and supports findings in published data of different cells like e.g. osteoclasts[72,73]. Here, these upstream regulators were proven to be important for podosome formation and degradation of ECM.

$Syk^{-/-}$ MKs on fibrinogen likewise confirmed the pharmacological findings, whereas $Syk^{-/-}$ MKs on collagen I reacted non-uniform. $Syk^{-/-}$ MKs obtained by lineage depletion, as well as WT MKs treated with the Syk inhibitor R406, reacted similarly as suggested by literature[74,75] and exhibited strongly reduced podosome formation and cell spreading. By contrast, MKs obtained by the enrichment method showed normal podosome formation despite Syk-loss. This observation can currently not be explained. MKs cultivated with the MK enrichment method are strongly increased in size and ploidy and thus, judging on these characteristics, might be more mature. However, the increased time of culture until analysis of the cells (6 days compared to 4 days of MKs obtained by lineage depletion) might affect MK characteristics. In this regard, it can at present not be excluded that Syk expression was to some extent restored in the fl/fl PF4-Cre expressing MKs, since according Western blots have not yet been performed. Ultimately, it is clear that results gained from cultured MKs cannot be easily compared and transferred to the physiological situation of MKs maturing in their local BM environment[76].

Src kinases and Syk are downstream effectors of platelet activation induced by the major collagen receptor GPVI. The involvement of GPVI in podosome formation on collagen I and fibrinogen was analyzed using MKs from $Gp6^{-/-}$ mice. While podosome formation on collagen I was not affected in $Gp6^{-/-}$ MKs, spreading was strongly reduced indicating that the GPVI signaling pathway is

active in mature MKs and can be induced by collagen I. Normal podosome formation and spreading on fibrinogen was somehow expected, as this substrate primarily induces outside-in signaling of active αIIbβ3[77].

Together, these data indicate that collagen I-induced MK podosome formation and spreading are regulated by different signaling pathways, only the latter one involving GPVI. Thus, it seems likely that integrin α2β1 is the major receptor inducing collagen-activated podosome formation, or maybe compensates for the loss of GPVI.

It should be noted that a recent study from our group supports the hypothesis that collagen I binding to GPVI on MKs induces inhibitory signaling to prevent premature PPF in the BM compartment via Src kinases but not Syk[78]. Using fetal liver cell derived MKs they observed that WT PPF was inhibited on collagen I. This inhibition was overcome in *Gp6*^{-/-} MKs and WT MKs treated with PP2 Src kinase inhibitor on collagen I, whereas it was not affected by Syk deficiency.

In summary, while the respective experimental conditions in the studies significantly impacted the observed results, they together indicate a role for GPVI in the process of platelet biogenesis. Further detailed studies using not only *in vitro* but also *in vivo* experiments will be required to dissect the complex GPVI signaling mechanism in MKs.

In the light of the proposed role for matrix metalloproteinase in MK podosome formation, MK-induced ECM degradation was investigated. In line with previous results[29], we could observe degradation of fluorescently labeled fibrinogen under podosome-forming MKs. Furthermore, accumulation of fluorescent signals in proximity to degraded areas might indicate that the degraded fibrinogen is partially taken up by MKs. In our hands, broad spectrum MMP inhibitors showed no influence on fibrinogen degradation by either WT or *RhoA*^{-/-} MKs. This stands in contrast to the literature[29,79]. While the results shown here are still to some extent preliminary, they raise the question whether MK-induced degradation of ECM proteins involves additional proteinases beside MMPs.

5 REFERENCES

1. Tsakiris DA, Scudder L, Hodivala-Dilke K, Hynes RO, Coller BS. Hemostasis in the mouse (Mus musculus): a review. *Thromb Haemost*. 1999;81(2):177-188.

2. Patel SR, Hartwig JH, Italiano JE, Jr. The biogenesis of platelets from megakaryocyte proplatelets. *J Clin Invest*. 2005;115(12):3348-3354.

3. Yip J, Shen Y, Berndt MC, Andrews RK. Primary platelet adhesion receptors. *IUBMB Life*. 2005;57(2):103-108.

4. Jackson SP. Arterial thrombosis--insidious, unpredictable and deadly. *Nat Med*. 2011;17(11):1423-1436.

5. Bertozzi CC, Schmaier AA, Mericko P, et al. Platelets regulate lymphatic vascular development through CLEC-2-SLP-76 signaling. *Blood*. 2010;116(4):661-670.

6. Nurden AT. Platelets, inflammation and tissue regeneration. *Thromb Haemost*. 2011;105 Suppl 1:S13-33.

7. Wagner DD, Burger PC. Platelets in inflammation and thrombosis. *Arterioscler Thromb Vasc Biol*. 2003;23(12):2131-2137.

8. Buergy D, Wenz F, Groden C, Brockmann MA. Tumor-platelet interaction in solid tumors. *Int J Cancer*. 2012;130(12):2747-2760.

9. Ogawa M. Differentiation and proliferation of hematopoietic stem cells. *Blood*. 1993;81(11):2844-2853.

10. Iazvikov VV. [The "megakaryocytes" of the spleen]. *Biull Eksp Biol Med*. 1967;64(9):104-106.

11.   Sharma GK, Talbot IC. Pulmonary megakaryocytes: "missing link" between cardiovascular and respiratory disease? *J Clin Pathol*. 1986;39(9):969-976.

12.   Larsson J, Karlsson S. The role of Smad signaling in hematopoiesis. *Oncogene*. 2005;24(37):5676-5692.

13.   Schmitt A, Guichard J, Masse JM, Debili N, Cramer EM. Of mice and men: comparison of the ultrastructure of megakaryocytes and platelets. *Exp Hematol*. 2001;29(11):1295-1302.

14.   Chang Y, Bluteau D, Debili N, Vainchenker W. From hematopoietic stem cells to platelets. *J Thromb Haemost*. 2007;5 Suppl 1:318-327.

15.   Malara A, Currao M, Gruppi C, et al. Megakaryocytes contribute to the bone marrow-matrix environment by expressing fibronectin, type IV collagen, and laminin. *Stem Cells*. 2014;32(4):926-937.

16.   Lüllmann-Rauch R. Taschenlehrbuch Histologie. 2009:132,133, 277-280.

17.   Avecilla ST, Hattori K, Heissig B, et al. Chemokine-mediated interaction of hematopoietic progenitors with the bone marrow vascular niche is required for thrombopoiesis. *Nat Med*. 2004;10(1):64-71.

18.   Massberg S, Konrad I, Schurzinger K, et al. Platelets secrete stromal cell-derived factor 1alpha and recruit bone marrow-derived progenitor cells to arterial thrombi in vivo. *J Exp Med*. 2006;203(5):1221-1233.

19.   Ara T, Nakamura Y, Egawa T, et al. Impaired colonization of the gonads by primordial germ cells in mice lacking a chemokine, stromal cell-derived factor-1 (SDF-1). *Proc Natl Acad Sci U S A*. 2003;100(9):5319-5323.

20. Ma Q, Jones D, Borghesani PR, et al. Impaired B-lymphopoiesis, myelopoiesis, and derailed cerebellar neuron migration in CXCR4- and SDF-1-deficient mice. *Proc Natl Acad Sci U S A*. 1998;95(16):9448-9453.

21. Zheng H, Fu G, Dai T, Huang H. Migration of endothelial progenitor cells mediated by stromal cell-derived factor-1alpha/CXCR4 via PI3K/Akt/eNOS signal transduction pathway. *J Cardiovasc Pharmacol*. 2007;50(3):274-280.

22. Bleul CC, Fuhlbrigge RC, Casasnovas JM, Aiuti A, Springer TA. A highly efficacious lymphocyte chemoattractant, stromal cell-derived factor 1 (SDF-1). *J Exp Med*. 1996;184(3):1101-1109.

23. Welford AF, Biziato D, Coffelt SB, et al. TIE2-expressing macrophages limit the therapeutic efficacy of the vascular-disrupting agent combretastatin A4 phosphate in mice. *J Clin Invest*. 2011;121(5):1969-1973.

24. Bluteau D, Lordier L, Di Stefano A, et al. Regulation of megakaryocyte maturation and platelet formation. *J Thromb Haemost*. 2009;7 Suppl 1:227-234.

25. Stegner D, vanEeuwijk JMM, Angay O, et al. Thrombopoiesis is spatially regulated by the bone marrow vasculature. *Nat Commun*. 2017;8(1):127.

26. Zhang L, Orban M, Lorenz M, et al. A novel role of sphingosine 1-phosphate receptor S1pr1 in mouse thrombopoiesis. *J Exp Med*. 2012;209(12):2165-2181.

27. Hla T, Galvani S, Rafii S, Nachman R. S1P and the birth of platelets. *J Exp Med*. 2012;209(12):2137-2140.

28. Hoshino D, Branch KM, Weaver AM. Signaling inputs to invadopodia and podosomes. *J Cell Sci*. 2013;126(Pt 14):2979-2989.

29.   Schachtner H, Calaminus SD, Sinclair A, et al. Megakaryocytes assemble podosomes that degrade matrix and protrude through basement membrane. *Blood.* 2013;121(13):2542-2552.

30.   Schachtner H, Calaminus SD, Thomas SG, Machesky LM. Podosomes in adhesion, migration, mechanosensing and matrix remodeling. *Cytoskeleton (Hoboken).* 2013;70(10):572-589.

31.   Linder S. The matrix corroded: podosomes and invadopodia in extracellular matrix degradation. *Trends Cell Biol.* 2007;17(3):107-117.

32.   Di Martino J, Paysan L, Gest C, et al. Cdc42 and Tks5: a minimal and universal molecular signature for functional invadosomes. *Cell Adh Migr.* 2014;8(3):280-292.

33.   French DL. Megakaryocytes put a foot through the door. *Blood.* 2013;121(13):2379-2380.

34.   Manuel Fuentes and Joshua LaBaer University of Salamanca SaASU, USA; respectively. Proteomics: Targeted Technology, Innovations and Applications. 2014.

35.   Bustelo XR, Sauzeau V, Berenjeno IM. GTP-binding proteins of the Rho/Rac family: regulation, effectors and functions in vivo. *Bioessays.* 2007;29(4):356-370.

36.   Ellenbroek SI, Collard JG. Rho GTPases: functions and association with cancer. *Clin Exp Metastasis.* 2007;24(8):657-672.

37.   Thumkeo D, Watanabe S, Narumiya S. Physiological roles of Rho and Rho effectors in mammals. *Eur J Cell Biol.* 2013;92(10-11):303-315.

38.   Pleines I, Hagedorn I, Gupta S, et al. Megakaryocyte-specific RhoA deficiency causes macrothrombocytopenia and defective platelet activation in hemostasis and thrombosis. *Blood*. 2012;119(4):1054-1063.

39.   Chen F, Ma L, Parrini MC, et al. Cdc42 is required for PIP(2)-induced actin polymerization and early development but not for cell viability. *Curr Biol*. 2000;10(13):758-765.

40.   Pleines I, Eckly A, Elvers M, et al. Multiple alterations of platelet functions dominated by increased secretion in mice lacking Cdc42 in platelets. *Blood*. 2010;115(16):3364-3373.

41.   Lozzio CB, Lozzio BB. Human chronic myelogenous leukemia cell-line with positive Philadelphia chromosome. *Blood*. 1975;45(3):321-334.

42.   Lozzio BB, Lozzio CB, Bamberger EG, Feliu AS. A multipotential leukemia cell line (K-562) of human origin. *Proc Soc Exp Biol Med*. 1981;166(4):546-550.

43.   Sutherland JA, Turner AR, Mannoni P, McGann LE, Turc JM. Differentiation of K562 leukemia cells along erythroid, macrophage, and megakaryocyte lineages. *J Biol Response Mod*. 1986;5(3):250-262.

44.   Ogura M, Morishima Y, Ohno R, et al. Establishment of a novel human megakaryoblastic leukemia cell line, MEG-01, with positive Philadelphia chromosome. *Blood*. 1985;66(6):1384-1392.

45.   Jackson B, Peyrollier K, Pedersen E, et al. RhoA is dispensable for skin development, but crucial for contraction and directed migration of keratinocytes. *Mol Biol Cell*. 2011;22(5):593-605.

46.   Wu X, Quondamatteo F, Lefever T, et al. Cdc42 controls progenitor cell differentiation and beta-catenin turnover in skin. *Genes Dev*. 2006;20(5):571-585.

47. Lorenz V, Stegner D, Stritt S, et al. Targeted downregulation of platelet CLEC-2 occurs through Syk-independent internalization. *Blood*. 2015;125(26):4069-4077.

48. Bender M, May F, Lorenz V, et al. Combined in vivo depletion of glycoprotein VI and C-type lectin-like receptor 2 severely compromises hemostasis and abrogates arterial thrombosis in mice. *Arterioscler Thromb Vasc Biol*. 2013;33(5):926-934.

49. Cervero P, Panzer L, Linder S. Podosome reformation in macrophages: assays and analysis. *Methods Mol Biol*. 2013;1046:97-121.

50. Butler TM, Ziemiecki A, Friis RR. Megakaryocytic differentiation of K562 cells is associated with changes in the cytoskeletal organization and the pattern of chromatographically distinct forms of phosphotyrosyl-specific protein phosphatases. *Cancer Res*. 1990;50(19):6323-6329.

51. Sander JD, Joung JK. CRISPR-Cas systems for editing, regulating and targeting genomes. *Nat Biotechnol*. 2014;32(4):347-355.

52. Jinek M, Chylinski K, Fonfara I, Hauer M, Doudna JA, Charpentier E. A programmable dual-RNA-guided DNA endonuclease in adaptive bacterial immunity. *Science*. 2012;337(6096):816-821.

53. Inc. OT. Quick learning of CRISPR/Cas9.

54. Bharti S, Inoue H, Bharti K, et al. Src-dependent phosphorylation of ASAP1 regulates podosomes. *Mol Cell Biol*. 2007;27(23):8271-8283.

55. Zimmet J, Ravid K. Polyploidy: occurrence in nature, mechanisms, and significance for the megakaryocyte-platelet system. *Exp Hematol*. 2000;28(1):3-16.

56.   Roberts DE, McNicol A, Bose R. Mechanism of collagen activation in human platelets. *J Biol Chem*. 2004;279(19):19421-19430.

57.   WHO. The top 10 causes of death. 2014.

58.   Lopez AD, Mathers CD, Ezzati M, Jamison DT, Murray CJ. Global and regional burden of disease and risk factors, 2001: systematic analysis of population health data. *Lancet*. 2006;367(9524):1747-1757.

59.   Feigin VL, Lawes CM, Bennett DA, Anderson CS. Stroke epidemiology: a review of population-based studies of incidence, prevalence, and case-fatality in the late 20th century. *Lancet Neurol*. 2003;2(1):43-53.

60.   Stoll G, Kleinschnitz C, Nieswandt B. Molecular mechanisms of thrombus formation in ischemic stroke: novel insights and targets for treatment. *Blood*. 2008;112(9):3555-3562.

61.   Nurden AT. Glanzmann thrombasthenia. *Orphanet J Rare Dis*. 2006;1:10.

62.   Lanza F. Bernard-Soulier syndrome (hemorrhagiparous thrombocytic dystrophy). *Orphanet J Rare Dis*. 2006;1:46.

63.   Brown DL. Congenital bleeding disorders. *Curr Probl Pediatr Adolesc Health Care*. 2005;35(2):38-62.

64.   Akbar H, Kim J, Funk K, et al. Genetic and pharmacologic evidence that Rac1 GTPase is involved in regulation of platelet secretion and aggregation. *J Thromb Haemost*. 2007;5(8):1747-1755.

65.   Dutting S, Gaits-Iacovoni F, Stegner D, et al. A Cdc42/RhoA regulatory circuit downstream of glycoprotein Ib guides transendothelial platelet biogenesis. *Nat Commun*. 2017;8:15838.

66. Yamazaki Y, Sanokawa R, Fujita Y, et al. Cytoplasmic elongation and rupture in megakaryoblastic leukemia cells via activation of adhesion and motility by staurosporine on fibronectin-bound substratum. *J Cell Physiol*. 1999;179(2):179-192.

67. Chen Z, Naveiras O, Balduini A, et al. The May-Hegglin anomaly gene MYH9 is a negative regulator of platelet biogenesis modulated by the Rho-ROCK pathway. *Blood*. 2007;110(1):171-179.

68. Malara A, Abbonante V, Di Buduo CA, Tozzi L, Currao M, Balduini A. The secret life of a megakaryocyte: emerging roles in bone marrow homeostasis control. *Cell Mol Life Sci*. 2015;72(8):1517-1536.

69. Vega FM, Fruhwirth G, Ng T, Ridley AJ. RhoA and RhoC have distinct roles in migration and invasion by acting through different targets. *J Cell Biol*. 2011;193(4):655-665.

70. Suzuki A, Shin JW, Wang Y, et al. RhoA is essential for maintaining normal megakaryocyte ploidy and platelet generation. *PLoS One*. 2013;8(7):e69315.

71. Palazzo A, Bluteau O, Messaoudi K, et al. The cell division control protein 42-Src family kinase-neural Wiskott-Aldrich syndrome protein pathway regulates human proplatelet formation. *J Thromb Haemost*. 2016;14(12):2524-2535.

72. Faccio R, Teitelbaum SL, Fujikawa K, et al. Vav3 regulates osteoclast function and bone mass. *Nat Med*. 2005;11(3):284-290.

73. Georgess D, Machuca-Gayet I, Blangy A, Jurdic P. Podosome organization drives osteoclast-mediated bone resorption. *Cell Adh Migr*. 2014;8(3):191-204.

74. Alexandra Mazharian, Steve G. Thomas, Tarvinder S. Dhanjal, Steve P. Watson, et al. Critical role of Src-Syk-PLCγ2 signaling in megakaryocyte migration and thrombopoiesis. *Blood.* 2010; 116: 793-800

75. J. C. Spalton, J. Mori, A. Y. Pollitt, C. E. Hughes, S. P. Watson, et al. The novel Syk inhibitor R406 reveals mechanistic differences in the initiation of GPVI and CLEC-2 signaling in platelets. *J Thromb Haemost. 2009, 7: 1192-1199*

76. Mazur EM, Basilico D, Newton JL, et al. Isolation of large numbers of enriched human megakaryocytes from liquid cultures of normal peripheral blood progenitor cells. *Blood.* 1990;76(9):1771-1782.

77. Larson MK, Watson SP. Regulation of proplatelet formation and platelet release by integrin alpha IIb beta3. *Blood.* 2006;108(5):1509-1514.

78. Semeniak D, Kulawig R, Stegner D, et al. Proplatelet formation is selectively inhibited by collagen type I through Syk-independent GPVI signaling. *J Cell Sci.* 2016;129(18):3473-3484.

79. Lane WJ, Dias S, Hattori K, et al. Stromal-derived factor 1-induced megakaryocyte migration and platelet production is dependent on matrix metalloproteinases. *Blood.* 2000;96(13):4152-4159.

6 APPENDIX

6.1 Abbreviations

BM	bone marrow
°C	degree Celsius
CD	cluster of differentiation
CFU	colony-forming units
DMEM	Dulbecco/Vogt Modified Eagle's Minimal Essential Medium
DMS	demarcation membrane system
ECL	enhanced Chemiluminescence
ECM	extracellular matrix
et al.	et alteri
F-actin	filamentous actin
f.c.	final concentration
FCS	fetal calf (bovine) serum
Fg	fibrinogen
Fig.	figure
FITC	fluorescein isothiocyanate
FSC	foreward scatter
g	gramme
GAP	GTPase-activating protein
GDP	guanosine diphosphate
GEF	guanine nucleotide exchange factor
GP	glycoprotein
GPCR	G protein-coupled receptor
GTP	guanosine trisphosphate
h	hour(s)
HRP	horseradish peroxidase
HSC	hematopoietic stem cell
H2O	water

IMDM	Iscove's Modified Dulbecco's Medium
IP	immunoprecipitation
kDa	kilo Dalton
l	litre
M	molar
MFI	mean fluorescence intensity
min	minute(s)
MK	megakaryocyte
mm	millimetre
μ	micro
MTOC	microtubule orientation center
NaCl	sodium chloride
NaOH	sodium hydroxide
o/n	overnight
PAA	polyacrylamide
PBM	peritoneal basement membrane
PBS	phosphate buffered saline
PMA	phorbol 12 myristate 13 acetate
PPF	proplatelet formation
PVDF	polyvinylidene difluoride
rpm	rounds per minute
RT	room temperature
s	second(s)
SD	standard deviation
SDF	stromal cell-derived factor
SSC	sideward scatter
Syk	spleen tyrosine kinase
TF	tissue factor
TPO	thrombopoietin

vWF	von Willebrand factor
WASP	Wiscott-Aldrich syndrome protein
WT	wildtype
x g	acceleration of gravity (9.81 m/ s²)

6.2 Acknowledgments

The here presented thesis was accomplished in the group of Professor Dr. Bernhard
Nieswandt, Chair of Vascular Medicine, Rudolf-Virchow-Center for Experimental Biomedicine, Julius-Maximilians-Universität Würzburg.

I would like to thank the following people for their help and support during the period of my MD work from August 2014 until August 2015.

- My doctorate supervisor Professor Dr. Bernhard Nieswandt for enabling me to work on this thesis.

- My senior Sebastian Dütting for all the help, support and teaching. Without him, I would never have learned enough to successfully accomplish this work.

- Professor Dr. Katrin Heinze, Professor Dr. Christoph Kleinschnitz and Professor Dr. Antje Gohla for being part of my thesis committee.

- The Graduate School of Life Sciences (GSLS) for funding my MD project.

- Professor Dr. Katrin Heinze and her team of the Bioimaging center for enabling me to work with confocal microscopy.

- All lab members who supported and helped me (a dentist in a biomedical laboratory needs a lot of help), especially Irina, Sylvia, Dominic, Judith, Max, Katja, Tobias and Simon.

Finally, I want to thank my family and friends.

6.3 Curriculum Vitae

Name	Frank Ottmar Gerner
Date of birth	02.03.1989
Place of birth	Hanau
Nationality	German

Work experience

From 8/2015 — Dentist in the practice of Dr. med. dent M.Sc. Oliver Maierhofer, Düsseldorf

Postgraduate education

08/2014 - 08/2015 — Medical thesis in the group of Professor Dr. Bernhard Nieswandt, Chair of Vascular Medicine, Rudolf-Virchow-Center for Experimental Biomedicine, Julius-Maximilians-Universität Würzburg

University education

06/2014 — Graduation: *Zahnmedizinisches Staatsexamen*

04/2009 - 06/2014 — Study of dentistry, Faculty of Medicine, Julius-Maximilians-Universität Würzburg

National service

08/2008 - 04/2009 — OP-assistant, Main-Kinzig-Kliniken, Gelnhausen

School education

2008 — German high school diploma: *Abitur* Kopernikussschule Freigericht, Germany

Düsseldorf, 06/12/2017 _____

Place, Date, Signature

6.4 Affidavit

I hereby confirm that my thesis entitled 'Functional analysis of polarization and podosome formation of murine and human megakaryocytes' is the result of my own work. I did not receive any help or support from commercial consultants. All sources and/or materials applied are listed and specified in the thesis.

Furthermore, I confirm that this thesis has not yet been submitted as part of another examination process neither in identical nor in similar form.

Düsseldorf, 06/12/2017   _____

Place, Date, Signature

6.5 Eidesstattliche Erklärung

Hiermit erkläre ich an Eides statt, die Dissertation „Funktionale Untersuchungen von Polarisation und Podosomenbildung von murinen und humanen Megakaryozyten" eigenständig, d.h. insbesondere selbständig und ohne Hilfe eines kommerziellen Promotionsberaters, angefertigt und keine anderen als die von mir angegebenen Quellen und Hilfsmittel verwendet zu haben.

Ich erkläre außerdem, dass die Dissertation weder in gleicher noch in ähnlicher Form bereits in einem anderen Prüfungsverfahren vorgelegen hat.

Düsseldorf, 06/12/2017   _____

Ort, Datum, Unterschrift